We are IntechOpen, the world's leading publisher of Open Access books Built by scientists, for scientists

4,800
Open access books available

122,000
International authors and editors

135M
Downloads

Our authors are among the

154
Countries delivered to

TOP 1%
most cited scientists

12.2%
Contributors from top 500 universities

CLARIVATE ANALYTICS BOOK CITATION INDEX INDEXED

WEB OF SCIENCE™

Selection of our books indexed in the Book Citation Index in Web of Science™ Core Collection (BKCI)

Interested in publishing with us?
Contact book.department@intechopen.com

Numbers displayed above are based on latest data collected.
For more information visit www.intechopen.com

7

Thermal Aspects of Conventional and Alternative Fuels in SuperCritical Water-Cooled Reactor (SCWR) Applications

Wargha Peiman, Igor Pioro and Kamiel Gabriel
University of Ontario Institute of Technology
Canada

1. Introduction

The demand for clean, non-fossil based electricity is growing; therefore, the world needs to develop new nuclear reactors with higher thermal efficiency in order to increase electricity generation and decrease the detrimental effects on the environment. The current fleet of nuclear power plants is classified as Generation III or less. However, these models are not as energy efficient as they should be because the operating temperatures are relatively low. Currently, a group of countries have initiated an international collaboration to develop the next generation of nuclear reactors called Generation IV. The ultimate goal of developing such reactors is to increase the thermal efficiency from what currently is in the range of 30 - 35% to 45 - 50%. This increase in thermal efficiency would result in a higher production of electricity compared to current Pressurized Water Reactor (PWR) or Boiling Water Reactor (BWR) technologies.

The Generation IV International Forum (GIF) Program has narrowed design options of the nuclear reactors to six concepts. These concepts are Gas-cooled Fast Reactor (GFR), Very High Temperature Reactor (VHTR), Sodium-cooled Fast Reactor (SFR), Lead-cooled Fast Reactor (LFR), Molten Salt Reactor (MSR), and SuperCritical Water-cooled Reactor (SCWR). These nuclear-reactor concepts differ in their design in aspects such as the neutron spectrum, coolant, moderator, and operating temperature and pressure.

A SuperCritical Water-cooled Reactor can be designed as a thermal-neutron-spectrum or fast-neutron-spectrum system. SCWR operates above the critical point of water which is at a temperature of 374°C and a pressure of 22.1 MPa. The operating pressure of SCWR is 25 MPa and the outlet temperature of the coolant is 550 - 625°C depending on the design chosen by the respective country that is developing it. The primary choice of fuel for SCWR is an oxide fuel while a metallic fuel has been considered as the secondary choice for the fast-neutron-spectrum SCWRs. A supercritical-water Rankine cycle has been chosen as the power cycle (US DOE, 2002). The thermal efficiency of SCWR is in the range of 45 – 50 %. Figure 1 shows a schematic diagram of a SCWR.

Some of the advantages of SCW Nuclear Power Plants (NPPs) over the conventional NPPs include higher thermal efficiency within a range of 45−50% (Pioro and Duffey, 2007) compared to 30 – 35% for the current NPPs, lower capital costs per kWh of electricity, and the possibility

for co-generation of hydrogen. For instance, the copper-chlorine cycle requires steam at temperatures between 500 and 530°C (Naterer et al., 2009, 2010), which is within the operating range of some SCWR designs. These systems work when supercritical water from a reactor flows through a heat exchanger and transfers heat to a low-pressure steam, which becomes a superheated steam. This superheated steam is transferred at the outlet of the heat exchanger to an adjacent hydrogen plant at a lower pressure (Naterer et al., 2009, 2010).

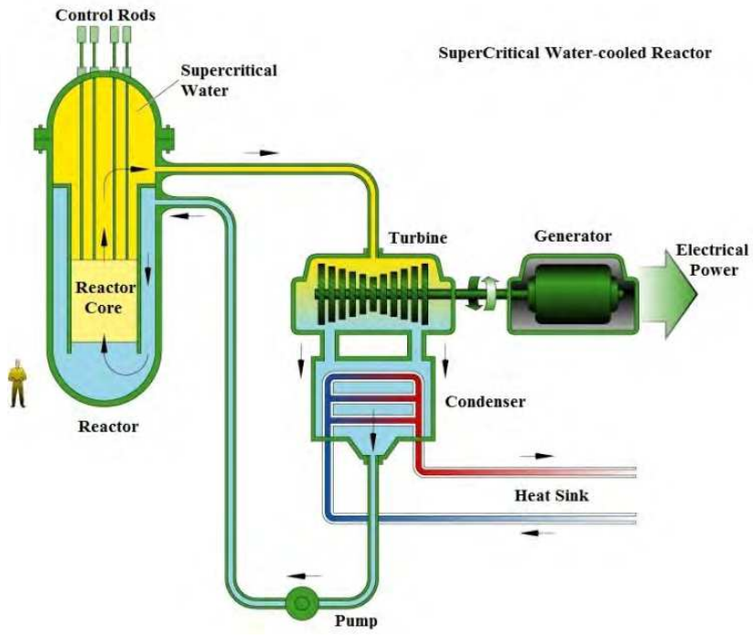

Fig. 1. Schematic diagram of PV SCWR (US DOE, 2002).

In general, SCWRs can be classified based on the neutron spectrum, moderator, or pressure boundary. In terms of the pressure boundary, SCWRs are classified into two categories, a) Pressure Vessel (PV) SCWRs, and b) Pressure Tube (PT) or Pressure Channel (PCh) SCWRs (Oka et al., 2010; Pioro and Duffey, 2007). The PV SCWR requires a thick pressure vessel with a thickness of about 50 cm (Pioro and Duffey, 2007) in order to withstand high pressures. The vast majority of conventional PWRs and BWRs are examples of PV reactors. Figure 1 shows a schematic diagram of a PV SCWR. On the other hand, the core of a PT SCWR consists of distributed pressure channels, with a thickness of 10 - 15 mm, which might be oriented vertically or horizontally, analogous to RBMK and CANDU reactors, respectively. For instance, SCW CANDU (CANada Deuterium Uranium) reactor consists of 300 horizontal fuel channels with coolant inlet and outlet temperatures of 350 and 625°C at a pressure of 25 MPa (Pioro and Duffey, 2007). It should be noted that a vertical core option has not been ruled out; both horizontal and vertical cores are being studied by the Atomic Energy of Canada Limited (AECL) (Diamond, 2010). Nevertheless, PT SCWRs provide a better control of flow and density variations. On the other hand, in PV SCWRs, there is a non-uniform temperature variation of coolant at the outlet of the pressure vessel.

In terms of the neutron spectrum, most SCWR designs are thermal-spectrum; however, fast-spectrum SCWR designs are studied. Recently, Liu et al. (2010) have proposed a mixed spectrum SCWR core, which consists of fast and thermal regions. In general, various solid or

liquid moderator options can be utilized in thermal-spectrum SCWRs. These options include light-water, heavy-water, graphite, beryllium oxide, and zirconium hydride (Kirillov et al., 2007). This liquid moderator concept can be used in both PV and PT SCWRs. The only difference is that in a PV SCWR, the moderator and the coolant are the same fluid. Thus, light-water is a practical choice for the moderator. In contrast, in PT SCWRs the moderator and the coolant are separated. As a result, there are a variety of options in PT SCWRs, mostly due to the separation of the coolant and the moderator.

One of these options is to use a liquid moderator such as light-water or heavy-water. One of the advantages of using a liquid moderator in PT SCWRs is that the moderator acts as a passive heat sink in the event of a Loss Of Coolant Accident (LOCA). A liquid moderator provides an additional safety feature[1], which enhances the safety of operation. On the other hand, one disadvantage of liquid moderators is an increased heat loss from the fuel channels to the liquid moderator, especially at SCWR conditions.

The second option is to use a solid moderator. Currently, in RBMK reactors and some other types of reactors such as AGR and HTR, graphite is used as the moderator. However, graphite may catch fire at high temperatures under some conditions when exposed to water or oxygen. Other materials such as beryllium oxide and zirconium hydride may be used as solid moderators (Kirillov et al., 2007). In this case, heat losses are reduced significantly. On the contrary, the solid moderators do not provide a passive-safety feature.

High operating temperatures of SCWRs leads to high fuel centerline temperatures. Currently, UO_2 has been used in Light Water Reactors (LWRs) and Pressurized Heavy Water Reactors (PHWRs); however, it has a low thermal conductivity which may result in high fuel centerline temperatures. Previous studies (Grande et al., 2010; Pioro et al., 2010; Villamere et al., 2009) have shown that the fuel centerline temperatures could exceed the industry limit of 1850°C (Reisch, 2009) when UO_2 is used at SCWR conditions. These studies have been conducted based on an average thermal power per channel and have not taken into account the effects of fuel-sheath gap on the sheath and fuel centreline temperatures. Additionally, the possibility of using enhanced thermal-conductivity fuels in SCWRs has not been examined by previous studies. Moreover, previous studies have focused on the fuel without any emphasis on the fuel channel. Therefore, there is a need to investigate the potential use of conventional and alternative fuels for future use in SCWRs.

2. Heat transfer at supercritical conditions

Heat transfer at supercritical conditions is characterized by changes in the thermophysical properties of the fluid specifically at pseudocritical points. A pseudocritical point exists at a pressure above the critical pressure of a fluid and at a temperature corresponding to the maximum value of the specific heat for this particular pressure (Pioro and Duffey, 2007). The increase in the specific heat reaches its maximum at the critical point and then decreases as the pressure increases. Furthermore, the pseudocritical temperature increases as the pressure increases. For instance, the corresponding pseudocritical temperatures of light-water at 23 and 25 MPa are approximately 377.5 and 384.9°C, respectively. Nevertheless, as the temperature passes through the pseudocritical temperature, the specific heat increases. This increase in the specific heat of the fluid allows for the deposition of a significant

[1]Currently, such option is used in CANDU-6 reactors.

amount of heat into the fluid. Eventually, this deposited heat can be converted into mechanical energy in steam turbines.

In addition to the specific heat, other thermophysical properties of a fluid undergo significant changes at the pseudocritical point. These changes affect the heat transfer capabilities of the fluid. Therefore, it is important to ensure that the thermophysical properties of a supercritical fluid are determined with accuracy. Figure 2 shows density and specific heat of water at 22.064 and 25 MPa. These thermophysical properties of water have been determined using the NIST REFPROP software.

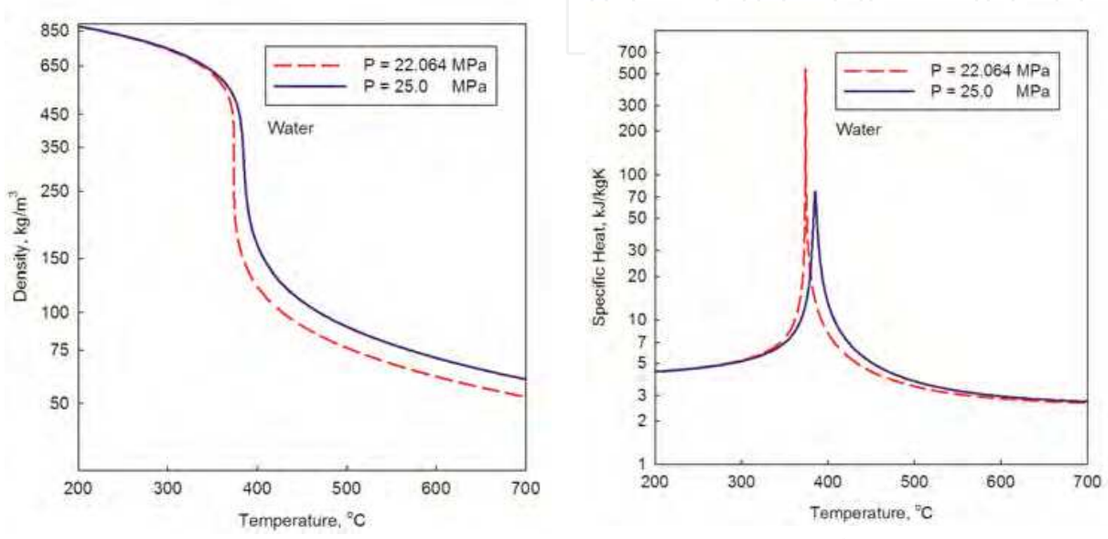

Fig. 2. a) Density and b) specific heat of water at 22.064 and 25 MPa.

In general, all thermophysical properties experience considerable changes near the critical and pseudocritical points. These changes are the greatest near the critical point; whereas, they become more gradual in the vicinity of the pseudocritical point. This gradual change in the thermophysical peroperties of fluids results in asingle-phase flow at supercritical conditions. In contrast, at subcritical conditions, a two-phase flow exists as the temperature of the fluid reaches the saturation temperature corresponding to the operating pressure. At the saturation tempertaure, the fluid undergoes a phase change from liquid to vapor when heat is added to the fluid. As a result of this phase change, there is a discontinuity in the variation of the thermophysical properties of the fluid. Figure 3a shows the density of water at 7, 11, and 15 MPa pressures, which correspond to the operating pressures of BWRs, CANDU reactors, and PWRs. As shown in Fig. 3a, there is a sharp drop in the density of water as the saturation temperatures of the corresponding pressures are reached.

The thermal efficiency of a Nuclear Power Plant (NPP) to a large extent depends on the pressure and temperature of the steam at the inlet to the turbine when the Rankine cycle is considered. In the case of either a direct cycle or an indirect cycle, the physical properties of the steam at the inlet of the turbine depend on the operating temperature and pressure of the reactor coolant. Figure 3b shows the operating pressures and temperatures of BWRs, PWRs, and PHWRs (e.g., CANDU reactors), which comprise the vast majority of the currently operating NPPs.

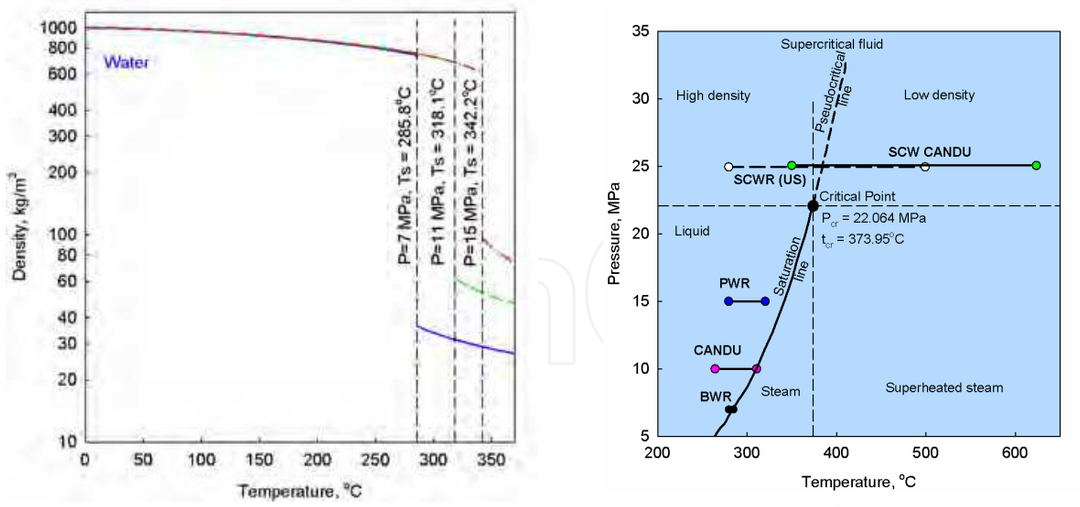

a b

Fig. 3. a) Density of water at 7, 11, and 15 MPa and b) Operating parameters of several reactors (Pioro and Duffey, 2007).

In terms of the operating conditions of the coolant, these reactors are all categorized as subcritical. PWRs have the highest operating pressure approximately at 15 MPa followed by CANDU reactors and BWRs, which operate at a pressure of 11 and 7 MPa, respectively. The outlet temperature of the coolant depends on the operating pressure of the reactor. In PWRs and CANDU reactors, the outlet temperature of the coolant is slightly below the saturation temperature of their corresponding operating pressures in order to avoid boiling of the coolant inside the reactor and achieve a high enthalpy rise across the reactor core. In addition, it is necessary to maintain the pressure within an operational margin due to pressure fluctuation during operation. As a result, the thermal efficiency of NPPs is limited by operating at subcritical pressures. Consequently, the operating pressure must be increased to pressures above the critical pressure in order to achieve higher thermal efficiencies compared to those of the current NPPs.

As shown in Fig. 3b, SCWRs operate at pressures and temperatures above the critical pressure and temperature of water. These high temperatures and pressures make it possible to use supercritical "steam" turbines, which have led to high thermal efficiencies when used in coal-fired power plants. As a result, SCWRs will use a proven technology, which has been examined over 50 years of operation in coal-fired power plants. The use of such technology minimizes the technological barriers for the development of suitable turbines for use in the SCW NPPs.

2.1 Heat-transfer correlations

The development of SCWRs requires an intensive study of convective heat transfer at supercritical pressures. Heat transfer at a supercritical pressure is different from that of a subcritical pressure because the thermophysical properties of a light-water coolant undergo significant variations as the temperature of the coolant passes through the pseudocritical point. Therefore, the traditional Nusselt number and other related non-dimensional parameters developed at subcritical pressures based on the bulk-fluid temperature cannot be used (Bae and Kim, 2009).

At a supercritical pressure, the thermophysical properties of a coolant at the sheath-wall temperature differ significantly from those at the bulk-fluid temperature. Although, a fluid does not undergo a phase change at a supercritical pressure, a low-density fluid separates the sheath-wall from a high-density fluid at high heat fluxes and low mass fluxes. This results in a reduction in the convective Heat Transfer Coefficient (HTC). Consequently, the sheath-wall temperature increases. This phenomenon is known as the Deteriorated Heat Transfer (DHT) regime. Therefore, the sheath-wall temperature must be reflected in a correlation, which is used to study the heat transfer at supercritical conditions.

Many correlations have been developed for the calculation of HTC at supercritical conditions. The most widely used correlations include those developed by Bishop et al. (1964); Swenson et al. (1965); Krasnoscheckov et al. (1967); Jackson (2002); and Mokry et al. (2009). Zahlan et al. (2011) compared the prediction capabilities of sixteen correlations including the aforementioned correlations. The conclusion of the Zahlan et al. (2011) comparison study showed that the Mokry et al. (2009) correlation resulted in the lowest Root-Mean-Square (RMS) error within the supercritical region compared to all other examined correlations.

3. Specifications of generic 1200-MW_{el} PT SCWR

The core of a generic 1200-MW_{el} PT SCWR consists of 300 fuel channels that are located inside a cylindrical tank called the calandria vessel. There are 220 SuperCritical-Water (SCW) fuel channels and 80 Steam Re-Heat (SRH) fuel channels. SRH and SCW fuel channels are located on the periphery and at the center of the core, respectively. In terms of neutron spectrum, the studied PT SCWR is a thermal-spectrum reactor. In this thermal-spectrum PT SCWR, light-water and heavy-water have been chosen as the coolant and the moderator, respectively. The coolant enters the supercritical fuel channels at an inlet temperature of 350°C and reaches an outlet temperature of 625°C at a pressure of 25 MPa. The inlet temperature of the SuperHeated Steam (SHS), which is used as the coolant, in the SRH fuel channels, is 400°C and the corresponding outlet temperature is 625°C at an operating pressure of 5.7 MPa. Table 1 lists the operating parameters of the generic 1200-MW_{el} PT SCWR (Naidin et al., 2009).

Parameters	**Unit**	**Generic PT SCWR**	
Electric Power	MW	1143-1270	
Thermal Power	MW	2540	
Thermal Efficiency	%	45 - 50	
Coolant/Moderator	-	H_2O/D_2O	
Pressure of SCW at Inlet | Outlet	MPa	25.8	25
Pressure of SHS at Inlet | Outlet	MPa	6.1	5.7
T_{in} | T_{out} Coolant (SCW)	°C	350	625
T_{in} | T_{out} Coolant (SHS)	°C	400	625
Mass Flow Rate per SCW|SRH Channel	kg/s	4.4	9.8
Thermal Power per SCW |SRH Channel	MW	8.5	5.5
# of SCW|SRH Channels	-	220	80

Table 1. Operating parameters of generic PT SCWR (Naidin et al., 2009).

3.1 Thermal cycles

The use of supercritical "steam" turbines in NPPs leads to higher thermal efficiencies compared to those of the current NPPs. There are several design options of Rankin cycles in order to convert the thermal energy of the supercritical "steam" into mechanical energy in a supercritical turbine. These design options include direct, indirect, and dual cycles. In a direct cycle, supercritical "steam" from the reactor passes directly through a supercritical turbine eliminating the need for the steam generators. This elimination reduces the costs and leads to higher thermal efficiencies compared to those produced in indirect cycles. In an indirect cycle, the supercritical coolant passes through the heat exchangers or steam generators to transfer heat to a secondary fluid, which passes through the turbine(s). The advantage of an indirect cycle is that potential radioactive particles would be contained inside the steam generators. On the other hand, the temperature of the secondary loop fluid is lower than that of the primary loop (e.g., reactor heat transport system loop). As a result, the thermal efficiency of an indirect cycle is lower than that of a direct cycle (Pioro et al., 2010). Figure 4 shows a single-reheat cycle for SCW NPPs.

With direct cycles, the thermal efficiency can be increased further through a combination of reheat and regeneration options. As shown in Fig. 4, in a single-reheat cycle, supercritical "steam" from the reactor passes through a high pressure turbine where its temperature and pressure drop. Then, the steam from the outlet of the high pressure turbine is sent through the SRH fuel channels inside the reactor core, but at a lower pressure. As the steam passes through the SRH fuel channels its temperature increases to an outlet temperature of 625°C at a pressure between 3 and 7 MPa (Pioro et al., 2010). At the outlet of the SRH channels, SHS passes through the intermediate pressure turbines. When a regenerative option is

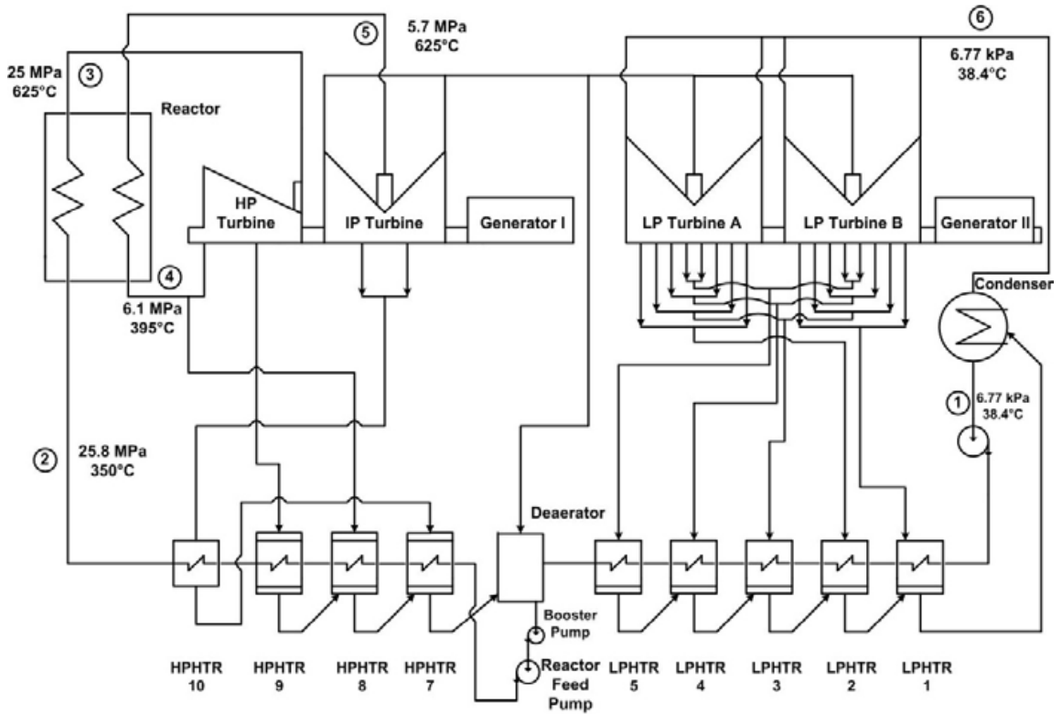

Fig. 4. Single-reheat cycle for SCW NPPs (Naidin et al., 2009).

considered, steam from high and intermediate turbines are extracted and sent to a series of open and closed feed-water heat exchangers. The steam is used to increase the temperature of the feed-water.

4. Fuel channel designs

The design of a fuel channel for SCWRs is an arduous undertaking due to high operating temperatures, which require materials that withstand temperatures as high as 625°C under normal operating conditions. In contrast, current materials, which withstand such design temperatures, have high absorption cross-sections for thermal neutrons. Consequently, a fuel-channel design must address the limitations due to material options to allow for maximum performance using available materials. AECL has proposed several fuel-channel designs for SCWRs. These fuel-channel designs can be classified into two categories: direct-flow and re-entrant channel concepts, which will be described in Sections 4.1 and 4.2. It should be noted that a re-entrant fuel-channel concept was developed by Russian scientists and was utilized at Unit 1 of the Beloyarskaya NPP in the 1960s (Saltanov et al., 2009).

4.1 High-Efficiency fuel Channel

The High Efficiency fuel Channel (HEC) consists of a pressure tube, a ceramic insulator, a liner tube, and fuel bundles. Figure 5 shows a 3-D view of HEC. The outer surface of the pressure tube is exposed to a moderator. The moderator could be a liquid moderator such as heavy-water or a solid moderator. The purpose of using an insulator is to reduce the operating temperature of the pressure tube and heat losses from the coolant to the moderator. Low operating temperatures of the pressure tube would allow for the use of available materials such as Zr-2.5%Nb, which has low absorption cross-sections for thermal neutrons (Chow and Khartabil, 2008).

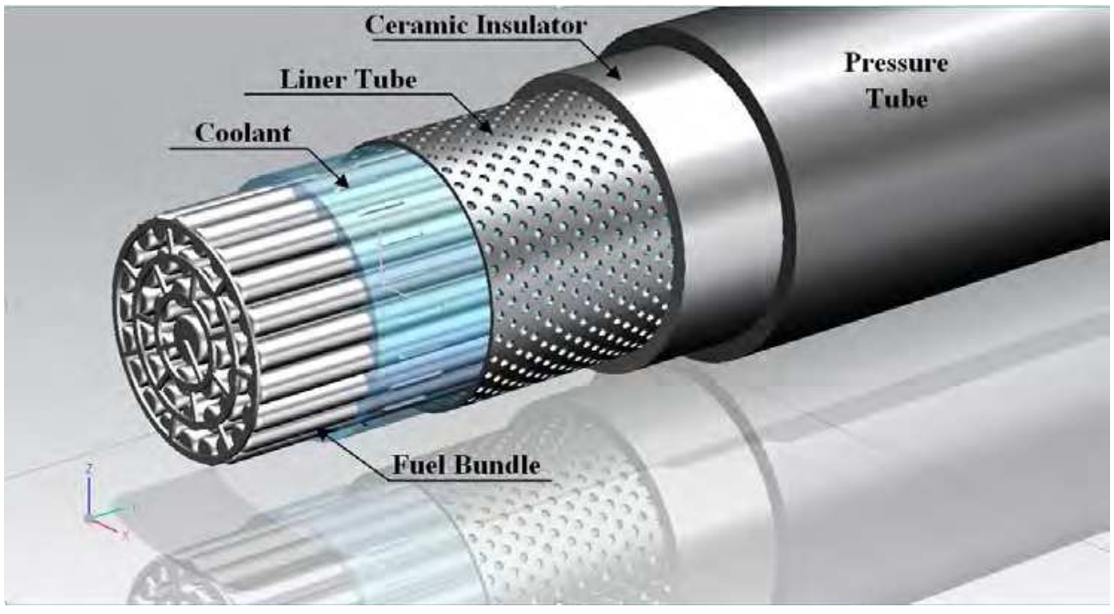

Fig. 5. High efficiency fuel channel (based on Chow and Khartabil, 2008).

The proposed material for the ceramic insulator is Yttria Stabilized Zirconia (YSZ) (Chow and Khartabil, 2008). YSZ has a low neutron absorption cross-section, low thermal-conductivity and high corrosion resistance in exposure to water at supercritical conditions (Chow and Khartabil, 2008). These properties make YSZ a good candidate as an insulator. The liner, which is a perforated tube and made of stainless steel, intends to protect the ceramic insulator from being damaged during operation or possible refuelling due to stresses introduced by fuel bundles and from erosion by the coolant flow.

4.2 Re-Entrant fuel Channels

There are several Re-Entrant fuel Channel (REC) designs. As shown in Fig. 6, the first design consists of a pressure tube and a flow tube which are separated by a gap. The coolant flows along the gap between the pressure tube and the flow tube. Then, at the end of the fuel channel, the coolant flows inside the flow tube where a bundle string is placed. The outer surface of the pressure tube is in contact with the moderator. The use of this fuel-channel design is possible only if the liquid moderator is pressurized to reduce heat loss.

Since the heat loss from the aforementioned fuel channel is significantly high, this design has been modified in the form of the fuel channels shown in Figs. 7 and 8. The second design (see Fig. 7) consists of a calandria tube, a pressure tube, and a flow tube. The gap between the pressure tube and the calandria tube is filled with an inert gas, which provides thermal insulation, reducing the heat losses from the 'hot' pressure tube to the moderator. As shown in Fig. 7, the outer surface of the calandria tube is exposed to a liquid moderator.

Unlike the HEC design, forces due to fuelling/refuelling are not exerted directly on the ceramic in the third design shown in Fig. 8, ensuring that the mechanical integrity of the ceramic insulator is maintained. In addition, the ceramic insulator acts as a thermal barrier, which in turn results in relatively lower operating temperatures of the pressure tube while reducing the heat loss from the coolant to the moderator. Such low operating temperatures allow for the use of Zr-2.5%Nb, which has low absorption cross-sections for thermal neutrons, as the material of the pressure tube. Therefore, lower heat losses, a better protection of the ceramic insulator, and the possibility of using Zr-2.5%Nb as the material of the pressure tube are several advantages of this fuel channel.

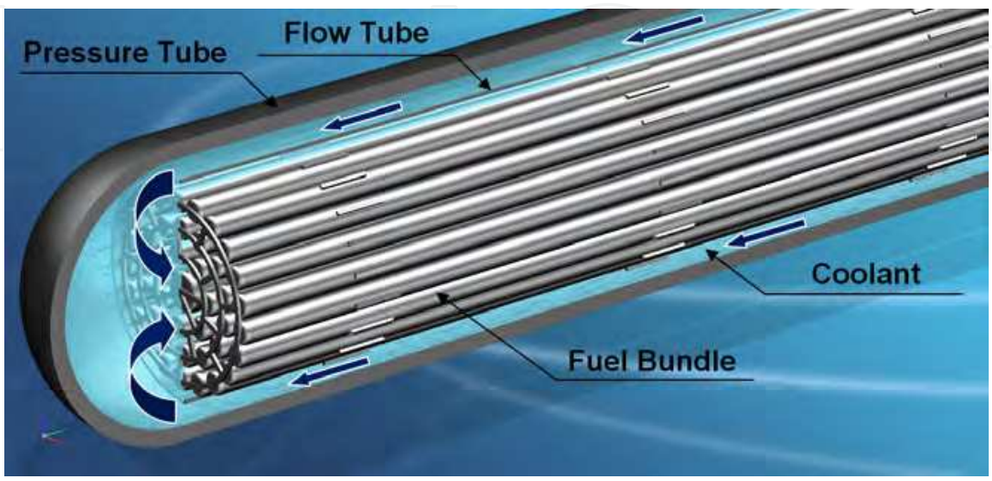

Fig. 6. Re-entrant fuel channel (based on Chow and Khartabil, 2008).

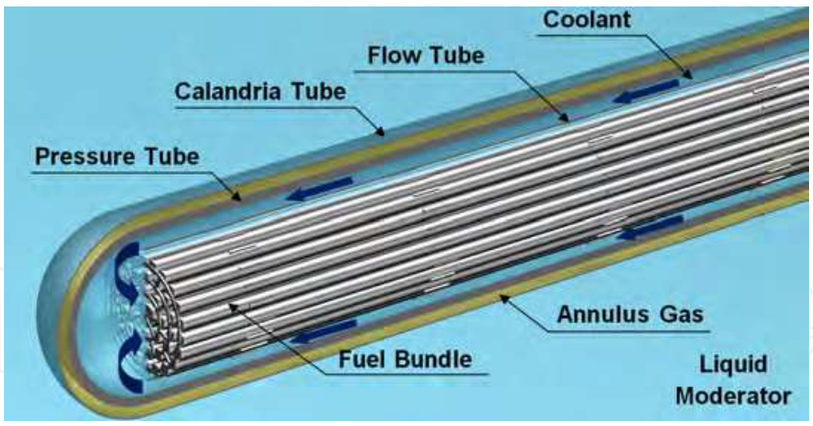

Fig. 7. Re-entrant fuel channel with gaseous insulator.

Fig. 8. Re-entrant fuel channel with ceramic insulator.

5. Nuclear fuels

Nuclear fuels can be classified into two main categories; metallic fuels and ceramic fuels. The most common metallic fuels include uranium, plutonium, and thorium (Kirillov et al., 2007). The advantage of metallic fuels is their high thermal conductivity; however, they suffer from low melting points and also that the fuel undergoes phase change. The three phases in a metallic uranium fuel includes α-, β-, and γ-phase. A phase changes to another phase as a function of temperature, resulting in a volume change in the fuel. In addition, metallic fuels undergo oxidation when exposed to air or water. For use in high-temperature applications, a potential fuel must have a high melting point, high thermal conductivity, and good irradiation and mechanical stability (Ma, 1983). These requirements eliminate various nuclear fuels categorized under the metallic fuels mainly due to their low melting points and high irradiation creep and swelling rates (Ma, 1983). On the other hand, ceramic fuels have promising properties, which make these fuels suitable candidates for SCWR applications. Table 2 provides basic properties of selected fuels at 0.1 MPa and 25°C (Chirkin, 1968; IAEA, 2008; Frost, 1963; Cox and Cronenberg, 1977; Leitnaker and Godfrey, 1967; Lundberg and Hobbins, 1992).

In general, ceramic fuels have good dimensional and radiation stability and are chemically compatible with most coolants and sheath materials. Consequently, this section focuses only

on ceramic fuels. The ceramic fuels examined in this chapter are UO_2, MOX, ThO_2, UC, UN, UO_2–SiC, UO_2–C, and UO_2–BeO. Further, these ceramic fuels can be classified into three categories: 1) low thermal-conductivity fuels, 2) enhanced thermal-conductivity fuels, and 3) high thermal-conductivity fuels. Low thermal-conductivity fuels are UO_2, MOX, and ThO_2. Enhanced thermal-conductivity fuels are UO_2-SiC, UO_2–C, and UO_2–BeO; and high thermal-conductivity fuels are UC and UN.

Property	**Unit**	**UO_2**	**MOX**	**ThO_2**	**UC**	**UN**
Molecular Mass	amu	270.3	271.2	264	250.04	252.03
Theoretical density	kg/m^3	10960	11,074	10,000	13630[2]	14420
Melting Point	°C	2847±30	2750	3227±150	2507[3] 2520 2532[4]	2850±30[5]
Heat Capacity	J/kgK	235	240	235	203[6]	190
Heat of Vaporization	kJ/kg	1530	1498	-	2120	1144[7] 3325[8]
Thermal Conductivity	W/mK	8.7	7.8	9.7	21.2	14.6
Linear Expansion Coefficient	1/K	9.75×10^{-6}	9.43×10^{-6}	$8.9^{9}\times10^{-6}$	10.1×10^{-6}	7.52×10^{-6}
Crystal Structure	-	FCC[10]	FCC	FCC	FCC	FCC

Table 2. Basic properties of selected fuels at 0.1 MPa and 25°C.

In addition to the melting point of a fuel, the thermal conductivity of the fuel is a critical property that affects the operating temperature of the fuel under specific conditions. UO_2 has been used as the fuel of choice in BWRs, PWRs, and CANDU reactors. The thermal conductivity of UO_2 is between 2 and 3 W/m K within the operating temperature range of SCWRs. On the other hand, fuels such as UC and UN have significantly higher thermal conductivities compared to that of UO_2 as shown in Fig. 9 (Cox and Cronenberg, 1977; Frost et al., 1963; IAEA, 2008; Ishimoto et al., 1995; Leitnaker and Godfrey, 1967; Khan et al., 2010, Kirillov et al., 2007; Lundberg and Hobbins, 1992; Solomon et al., 2005). Thus, under the same operating conditions, the fuel centerline temperature of high thermal conductivity fuels should be lower than that of UO_2 fuel.

[2] Frost(1963)
[3] Cox and Cronenberg (1977)
[4] Lundberg and Hobbins (1992)
[5] at nitrogen pressure ≥ 0.25 MPa
[6] Leitnaker & Godfrey (1967)
[7] UN(s)=U(l)+0.5N_2(g), Gingerich (1969)
[8] UN(s)=U(g)+0.5N_2(g), Gingerich (1969)
[9] at 1000°C, Bowman et al.(1965;1966)
[10] Faced-Centered Cubic (FCC)

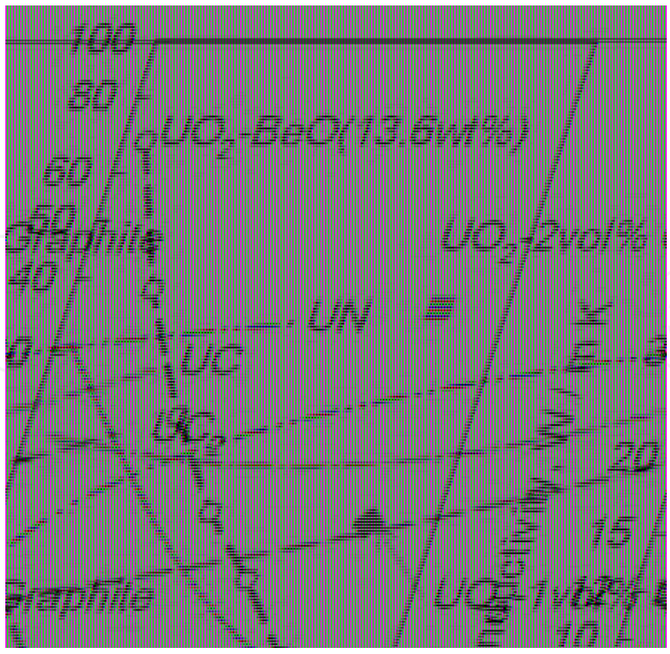

Fig. 9. Thermal conductivities of several fuels.

5.1 Low Thermal-Conductivity Fuels: UO_2, MOX, and ThO_2

5.1.1 UO_2 and MOX

As a ceramic fuel, Uranium Dioxide (UO_2) is a hard and brittle material due to its ionic or covalent interatomic bonding. In spite of that, the uranium dioxide fuel is currently used in PWRs, BWRs, and CANDU reactors because of its properties. Firstly, oxygen has a very low thermal-neutron absorption cross-section, which does not result in a serious loss of neutrons. Secondly, UO_2 is chemically stable and does not react with water within the operating temperatures of these reactors. Thirdly, UO_2 is structurally very stable. Additionally, the crystal structure of the UO_2 fuel retains most of fission products even at high burn-up (Cochran and Tsoulfanidis, 1999). Moreover, UO_2 has a high melting point; however, its thermal conductivity is very low, minimizing the possibility of using UO_2 as a fuel of choice for SCWRs. The thermal conductivity of 95% Theoretical Density (TD) UO_2 can be calculated using the Frank correlation, shown as Eq. (1) (Carbajo et al., 2001). This correlation is valid for temperatures in the range of 25 to 2847°C.

$$k_{uo_2}(T) = \frac{100}{7.5408 + 17.692\,(10^{-3}T) + 3.6142\,(10^{-3}T)^2} + \frac{6400}{(10^{-3}T)^{5/2}} \exp^{-16.35/(10^{-3}T)} \quad (1)$$

Mixed Oxide (MOX) fuel refers to nuclear fuels consisting of UO_2 and plutonium dioxide (PuO_2). MOX fuel was initially designed for use in Liquid-Metal Fast Breeder Reactors (LMFBRs) and in LWRs when reprocessing and recycling of the used fuel is adopted (Cochran and Tsoulfanidis, 1999). The uranium dioxide content of MOX may be natural, enriched, or depleted uranium, depending on the application of MOX fuel. In general, MOX fuel contains between 3 and 5% PuO_2 blended with 95 – 97 % natural or depleted uranium dioxide (Carbajo et al., 2001). The small fraction of PuO_2 slightly changes the thermophysical

properties of MOX fuel compared with those of UO_2 fuel. Nonetheless, the thermophysical properties of MOX fuel should be selected when a study of the fuel is undertaken.

Most thermophysical properties of UO_2 and MOX (3 – 5 % PuO_2) have similar trends. For instance, thermal conductivities of UO_2 and MOX fuels decrease as the temperature increases up to 1700°C (see Fig. 9). The most significant differences between these two fuels have been summarized in Table 2. Firstly, MOX fuel has a lower melting temperature, lower heat of fusion, and lower thermal conductivity than UO_2 fuel. For the same power, MOX fuel has a higher stored energy which results in a higher fuel centerline temperature compared with UO_2 fuel. Secondly, the density of MOX fuel is slightly higher than that of UO_2 fuel.

The thermal conductivity of the fuel is of importance in the calculation of the fuel centerline temperature. The thermal conductivities of MOX and UO_2 decrease as functions of temperature up to temperatures around 1527 – 1727°C, and then it increases as the temperature increases (see Fig. 9). In general, the thermal conductivity of MOX fuel is slightly lower than that of UO_2. In other words, addition of small amounts of PuO_2 decreases the thermal conductivity of the mixed oxide fuel. However, the thermal conductivity of MOX does not decrease significantly when the PuO_2 content of the fuel is between 3 and 15%. But, the thermal conductivity of MOX fuel decreases as the concentration of PuO_2 increases beyond 15%. As a result, the concentration of PuO_2 in commercial MOX fuels is kept below 5% (Carbajo et al., 2001). Carbajo et al. (2001) recommended the following correlation shown as Eq. (2) for the calculation of the thermal conductivity of 95% TD MOX fuel. This correlation is valid for temperatures between 427 and 2827°C, x less than 0.05, and PuO_2 concentrations between 3 and 15%. In Eq. (2), T indicates temperature in Kelvin.

$$k(T,x) = \frac{1}{A + C(10^{-3}T)} + \frac{6400}{(10^{-3}T)^{5/2}} \exp^{-16.35/(10^{-3}T)}, \quad x = 2 - O/M \tag{2}$$

Where x is a function of oxygen to heavy metal ration and

$$A(x) = 2.58x + 0.035 \quad (\mathrm{mK/W}), \quad C(x) = -0.715x + 0.286 \quad (\mathrm{m/K})$$

5.1.2 ThO_2

Currently, there is an interest in using thorium based fuels in nuclear reactors. Thorium is widely distributed in nature and is approximately three times as abundant as uranium. However, ThO_2 does not have any fissile elements to fission with thermal neutrons. Consequently, ThO_2 must be used in combination with a "driver" fuel (e.g., UO_2 or UC), which has ^{235}U as its initial fissile elements. The presence of a "driver" fuel such as UO_2 in a nuclear-reactor core results in the production of enough neutrons, which in turn start the thorium cycle. In this cycle, ^{232}Th is converted into ^{233}Th, which decays to ^{233}Pa. The latter element eventually results in the formation of ^{233}U, which is a fissile element (Cochran and Tsoulfanidis, 1999).

In regards to PT reactors, there are two possibilities when ThO_2 is used. One option is to place ThO_2 and a "driver" fuel in different fuel channels. The separation between ThO_2 fuel and the "driver" fuel allows ThO_2 fuel to stay longer inside the core. The second option is to

enclose ThO_2 and the "driver" in same fuel bundles, which are placed inside the fuel channels throughout the reactor core. This option requires the enrichment of the "driver" fuel since it has to be irradiated as long as ThO_2 fuel stays inside the core (IAEA, 2005). Nevertheless, the current study considers the thermal aspects of one single fuel channel, which consists of ThO_2 fuel bundles (i.e., first Option). However, this assumption does not suggest that the whole core is composed of fuel channels containing ThO_2.

The use of thorium based fuels in nuclear reactors requires information on the thermophysical properties of these fuels, especially thermal conductivity. Jain et al. (2006) conducted experiments on thorium dioxide (ThO_2). In their analysis, the thermal conductivity values were calculated based on Eq. (3), which requires the measured values of the density, thermal diffusivity, and specific heat of ThO_2. These properties were measured for temperatures between 100 and 1500°C (Jain et al., 2006). In the current study, the correlation developed by Jain et al. (2006), which is shown as Eq. (4), has been used.

$$k = a\rho c_p \tag{3}$$

$$k_{ThO_2} = \frac{1}{0.0327 + 1.603\times10^{-4} T} \tag{4}$$

5.2 High Thermal-Conductivity Fuels: UC and UN

5.2.1 UC

From a heat transfer point of view, there is an interest on carbides of uranium as nuclear fuels due to their high thermal conductivities and high melting points. Carbides of uranium usable for nuclear fuels are Uranium Carbide (UC) and Uranium Dicarbide (UC_2). For instance, UC has been proposed as the fuel of choice for a SCWR concept in Russia (Pioro and Duffey, 2007). Uranium sesquicarbide (U_2C_3) is another carbide of uranium; however, it cannot be manufactured through casting or compaction of a powder. However, UC_2 may transform to U_2C_3 at high temperatures and under stress (Frost, 1963).

UC, which has a Faced-Centered Cubic (FCC) crystal structure similar to those of UN and NaCl, has a high melting point approximately 2507°C and a high thermal conductivity, above 19 W/m K at all temperatures up to the melting point. UC has a density of 13630 kg/m^3, which is lower than that of UN but higher than those of UO_2. It should be noted that the density of hypo-stoichiometric UC is slightly higher than that of stoichiometric UC, which is listed in Table 2. Coninck et al. (1975) reported densities between 13730 and 13820 kg/m^3 at 25°C for hypo-stoichiometric UC. Moreover, UC has a higher uranium atom density compared to UO_2 but lower than that of UN. The uranium atom densities of UC and UN are 1.34 and 1.4 times that of UO_2, respectively.

For hypo-stoichiometric UC, the thermal diffusivity a, in m^2/s, and thermal conductivity k, in W/m K, correlations are valid for a temperature range of 570 and 2000°C. In Eqs. (5) and (6), T is in degrees Kelvin (Coninck et al., 1975). For stoichiometric UC, Coninck et al. (1975) provided two correlations, shown as Eqs. (7) and (8), which can be used to determine the mean values of the thermal diffusivity and thermal conductivity of stoichiometric UC for a temperature range between 850 and 2250°C, in m^2/s and W/m K, respectively.

$$\alpha = 10^{-4} \cdot \left[5.75 \cdot 10^{-2} + 1.25 \cdot 10^{-6} (T\text{-}273.15) \right] \quad (5)$$

$$k = 100 \cdot \left[2.04 \cdot 10^{-1} + 2.836 \cdot 10^{-8} (T - 843.15)^2 \right] \quad (6)$$

$$\alpha = 10^{-4} \cdot \left[5.7 \cdot 10^{-2} + 1.82 \cdot 10^{-12} (T\text{-}1123.15)^3 \right] \quad (7)$$

$$k = 100 \cdot \left[1.95 \cdot 10^{-1} + 3.57 \cdot 10^{-8} (T\text{-}1123.15)^2 \right] \quad (8)$$

In addition to Eqs. (6) and (8), Kirillov et al. (2007) have recommended another correlation, shown as Eqs. (9) and (10), for the calculation of the thermal conductivity of UC in W/m K. In the current study, Eq. (21) have been used to determine the thermal conductivity of UC for the calculation of the UC fuel centerline temperature at SCWR conditions, because this equation provides the lowest thermal conductivity values for a wide temperature range, leading to a conservative calculation of the fuel centerline temperature. In Eqs. (9) and (10), T is in degrees Kelvin.

$$k = 21.7 - 3.04 \cdot 10^{-3} (T\text{-}273.15) + 3.61 \cdot 10^{-6} (T\text{-}273.15)^2, \quad 323 < T < 973 \text{ K} \quad (9)$$

$$k = 20.2 + 1.48 \times 10^{-3} (T\text{-}273.15), \quad 973 < T < 2573 \text{ K} \quad (10)$$

Frost (1963) developed a correlation shown as Eq. (11), which can be used to determine the diametric increase of UC fuel as a function of time-averaged fuel centerline temperature. According to Eq. (11), UC fuel undergoes significant swelling for temperatures above 1000°C. In Eq. (11), R_D and T are percent diametric increase per atom % burn-up and time-averaged fuel centerline temperature in K, respectively. In addition, as shown in Fig. 10, Harrison (1969) provided the volumetric swelling of UC as a function of burn-up for various temperatures.

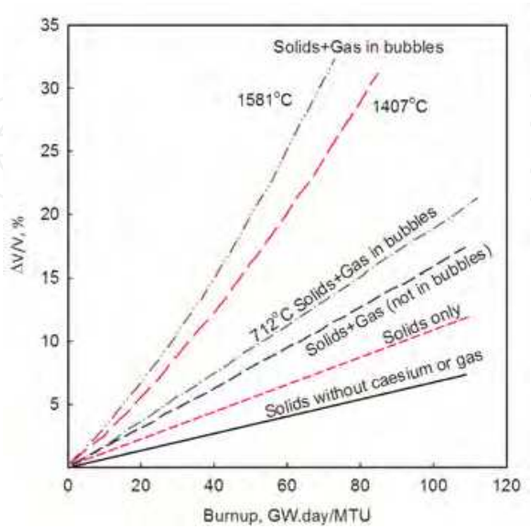

Fig. 10. Volumetric swelling of UC as function of temperature and burn-up.

$$R_D = 0.6 + 0.77\left(\frac{9 \cdot T}{5000} - 1\right) \tag{11}$$

5.2.2 UN

Uranium mononitride or uranium nitride (UN), which is a ceramic fuel, can be produced by the carbothermic reduction of uranium dioxide plus carbon in nitrogen. This process produces UN with densities in the range of 65 to 90% of TD (Shoup and Grace, 1977). UN has a high melting point, high thermal conductivity, and high radiation stability. These properties enhance the safety of operation and allow the fuel to achieve high burn-ups (IAEA, 2008). In addition, UN has the highest fissile atom density, which is approximately 1.4 times that of UO_2 and greater than those of other examined fuels. In other words, when UN is used as a fuel, a smaller volume of fuel is required, which leads to a smaller core. In contrast, one disadvantage of the UN fuel is that under some conditions it decomposes to liquid uranium and gaseous nitrogen (IAEA, 2008), which in turn results in the formation of cracks in the fuel. These cracks increase the chance of the release of gaseous fission products. In addition, the formation of cracks in nuclear fuels has adverse effects on their mechanical and thermophysical properties.

Hayes et al. (1990a) developed a correlation shown as Eq. (12), which calculates the thermal conductivity of UN, in W/m K. This correlation, which is a function of both temperature and percent porosity, can be applied when porosity changes between 0 and 20% for temperatures in the range of 25°C and 1650°C (Hayes et al., 1990a). The standard deviation of the Hayes et al. correlation is ±2.3%.

$$k = 1.864 \exp(-2.14\, P)\, T^{0.361} \tag{12}$$

Irradiation swelling, growth, and creep are the primary effects of irradiation on a nuclear fuel. Irradiation swelling results in volumetric instability of the fuel at high temperatures while irradiation growth causes dimensional instability of the fuel at temperatures lower than 2/3 of the melting point of the fuel (Ma, 1983). In addition to dimensional and volumetric instability, a continuous and plastic deformation of the fuel due to creep may adversely affect its mechanical properties. Thus, it is required to study the behaviour of the fuel under irradiation specifically the irradiation-induced swelling, irradiation-induced growth and irradiation-induced creep of the fuel.

Ross et al. (1990) developed a correlation for the prediction of percent volumetric swelling of UN fuel. This correlation is shown as Eq. (13), where T_{avg} is the volume average fuel temperature in K, B is the fuel burn-up in MW day/M g(U), and $\rho_{\%TD}$ is the percent theoretical density of the fuel (e.g., $\rho_{\%TD}$ equals to 0.95 for a fuel with 5% porosity). In addition to this correlation, the volumetric swelling of UN can be calculated based on fuel centerline temperature using Eq. (14) (Ross et al., 1990). The uncertainty associated with Eq. (14) is ±25% for burn-ups above 10,000 MW day/Mg (U) while at lower burn-ups the uncertainty increases to ±60% (Ross et al., 1990). Figure 11 shows the volume expansion of 95% TD UN based on Eq. (14).

$$\Delta V/V(\%) = 4.7 \cdot 10^{-11}\, T_{avg}^{3.12} \left(\frac{B}{9008.1}\right)^{0.83} \rho_{\%TD}^{0.5} \tag{13}$$

$$\Delta V/V(\%) = 1.16 \cdot 10^{-8}\, T_{CLT}^{2.36} \left(\frac{B}{9008.1} \right)^{0.82} \rho_{\%TD}^{0.5} \tag{14}$$

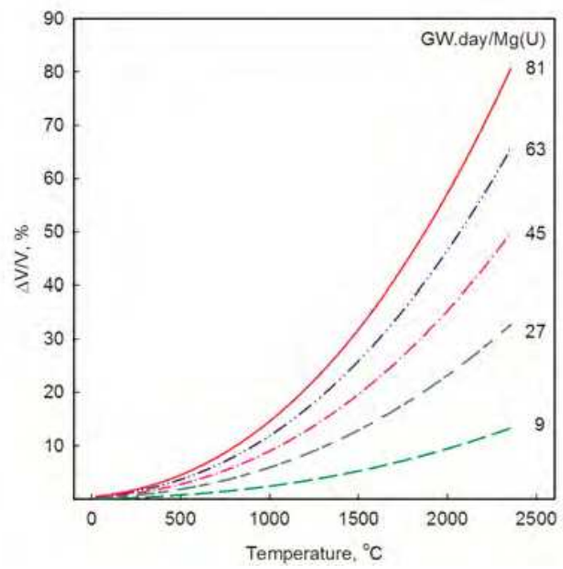

Fig. 11. Percent volumetric swelling of UN as function of burn-up and temperature.

5.3 Composite fuels with enhanced thermal-conductivity

Currently, there is a high interest in developing high thermal-conductivity fuels, and improving the thermal conductivity of low thermal-conductivity fuels such as UO_2. High thermal conductivities result in lower fuel centerline temperatures and limit the release of gaseous fission products (Hollenbach and Ott, 2010). As shown previously, UO_2 has a very low thermal conductivity at high temperatures compared to other fuels such as UC and UN. However, there is a possibility to increase the thermal conductivity of UO_2. This increase in the thermal conductivity of UO_2 can be performed either by adding a continuous solid phase or long, thin fibbers of a high thermal-conductivity material (Hollenbach and Ott, 2010; Solomon et al., 2005).

A high thermal-conductivity material must have a low thermal-neutron absorption cross-section, assuming that the fuel will be used in a thermal-spectrum nuclear reactor (Hollenbach and Ott, 2010). In addition, it must have a high melting point and be chemically compatible with the fuel, the cladding, and the coolant. The need to meet these requirements narrows the potential materials to silicon carbide (SiC), beryllium oxide (BeO), and graphite (C). The following sections provide some information about UO_2 fuel composed of the aforementioned high thermal-conductivity materials.

5.3.1 UO_2 - SiC

The thermal conductivity of UO_2 fuel can be improved by incorporating silicon carbide (SiC) into the matrix of the fuel. SiC has a high melting point approximately at 2800°C, high thermal conductivity (78 W/m K at 727°C), high corrosion resistance even at high temperatures, low

thermal neutron absorption, and dimensional stability (Khan et al., 2010). Therefore, when used with UO_2, SiC can address the problem of low thermal conductivity of UO_2 fuel.

Calculation of the thermal conductivity of UO_2 plus SiC the fuel falls under the theories of composites. Generally, theories contemplating the thermal conductivity of composites are classified into two categories. One category assumes that inclusions are randomly distributed in a homogeneous mixture. The effective thermal conductivities of the composites, based on the aforementioned principle, are formulated by Maxwell. The other category, which is based on the work performed by Rayleigh, assumes that particles are distributed in a regular manner within the matrix.

Khan et al. (2010) provided the thermal conductivity of UO_2–SiC fuel as a function of temperature and weight percent of SiC. Khan et al. (2010) assumed that the thin coat of SiC covered UO_2 particles and determined the thermal conductivity of the composite fuel for three cases. The results of the study conducted by Khan et al. (2010) indicate that the continuity of SiC layer leads to a relatively significant increase in thermal conductivity. However, the discontinuity of SiC resulted in little improvement in the ETC of the fuel. Thus, the addition of a continuous solid phase of SiC to UO_2 fuel increases the effective thermal conductivity of the fuel. In the present study, UO_2–SiC fuel with 12wt% SiC with an overall 97 percent TD has been examined and its thermal conductivity has been calculated using Eq. (15).

$$k_{\text{eff}} = -9.59 \cdot 10^{-9}\, T^3 + 4.29 \cdot 10^{-5}\, T^2 - 6.87 \cdot 10^{-2}\, T + 4.68 \cdot 10 \tag{15}$$

5.3.2 UO_2-C

Hollenbach and Ott (2010) studied the effects of the addition of graphite fibbers on thermal conductivity of UO_2 fuel. Theoretically, the thermal conductivity of graphite varies along different crystallographic planes. For instance, the thermal conductivity of perfect graphite along basal planes is more than 2000 W/m K (Hollenbach and Ott, 2010). On the other hand, it is less than 10 W/m K in the direction perpendicular to the basal planes. Hollenbach and Ott (2010) performed computer analyses in order to determine the effectiveness of adding long, thin fibbers of high thermal-conductivity materials to low thermal-conductivity materials to determine the effective thermal conductivity. In their studies, the high thermal-conductivity material had a thermal conductivity of 2000 W/m K along the axis, and a thermal conductivity of 10 W/m K radially, similar to perfect graphite. The low thermal-conductivity material had properties similar to UO_2 (e.g., with 95% TD at ~1100°C) with a thermal conductivity of 3 W/m K.

Hollenbach and Ott (2010) examined the effective thermal conductivity of the composite for various volume percentages of the high thermal-conductivity material, varying from 0 to 3%. The results show if the amount of the high thermal-conductivity material increases to 2 % by volume, the effective thermal conductivity of the composite reaches the range of high thermal-conductivity fuels, such as UC and UN.

5.3.3 UO_2–BeO

Beryllium Oxide (BeO) is a metallic oxide with a very high thermal conductivity. BeO is chemically compatible with water, UO_2, and most sheath materials including zirconium

alloys. In addition to its chemical compatibility, BeO is insoluble with UO_2 at temperatures up to 2160°C. As a result, BeO remains as a continuous second solid phase in the UO_2 fuel matrix while being in good contact with UO_2 molecules at the grain boundaries. BeO has desirable thermochemical and neutronic properties, which have resulted in the use of BeO in aerospace, electrical and nuclear applications. For example, BeO has been used as the moderator and the reflector in some nuclear reactors. However, the major concern with beryllium is its toxicity. But, the requirements for safe handling of BeO are similar to those of UO_2. Therefore, the toxicity of BeO is not a limiting factor in the use of this material with UO_2 (Solomon et al., 2005).

Similar to other enhanced thermal-conductivity fuels, the thermal conductivity of UO_2 can be increased by introducing a continuous phase of BeO at the grain boundaries. The effects of the present of such second solid phase on the thermal conductivity of UO_2 is significant such that only 10% by volume of BeO would improve the thermal conductivity of the composite fuel by 50% compared to that of UO_2 with 95% TD. For the purpose of this study, UO_2–BeO fuel with 13.6 wt% of BeO has been examined.

6. Fuel centerline temperature calculations

In order to calculate the fuel centerline temperature, steady-state one-dimensional heat-transfer analysis was conducted. The MATLAB and NIST REFPROP software were used for programming and retrieving thermophysical properties of a light-water coolant, respectively. First, the heated length of the fuel channel was divided into small segments of one-millimeter lengths. Second, the temperature profile of the coolant was calculated. Third, sheath-outer and inner surface temperatures were calculated. Fourth, the heat transfer through the gap between the sheath and the fuel was determined and used to calculate the outer surface temperature of the fuel. Finally, the temperature of the fuel in the radial and axial directions was calculated. It should be noted that the radius of the fuel pellet was divided into 20 segments. The results will be presented for fuel-sheath gap widths of zero, 20 μm and 36 μm. Moreover, the fuel centerline temperature profiles have been calculated based on a no-gap condition in order to determine the effect of gap conductance on the fuel centerline temperature. Figure 12 illustrates the methodology based on which fuel centerline temperature was calculated. The following section provides more information about each step shown in Fig. 12.

As shown in Fig. 12, the convective heat transfer between the sheath and the coolant is the only heat transfer mode which has been taken directly into consideration. In radiative heat transfer, energy is transferred in the form of electromagnetic waves. Unlike convection and conduction heat transfer modes in which the rate of heat transfer is linearly proportional to temperature differences, a radiative heat transfer depends on the difference between absolute temperatures to the fourth power. The sheath temperature is high[11] at SCWR conditions; therefore, it is necessary to take into account the radiative heat transfer.

In the case of the sheath and the coolant, the radiative heat transfer has been taken into consideration in the Nusselt number correlation, which has been used to calculate the HTC. In general, the Nusselt number correlations are empirical equations, which are developed

[11] It might be as high as 850°C.

based on experiments conducted in water using either bare tubes or tubes containing electrically heated elements simulating the fuel bundles. To develop a correlation, surface temperatures of the bare tube and/or simulating rods are measured along the heated length of the test section by the use of thermocouples or Resistance Temperature Detectors (RTDs). These measured surface temperatures already include the effect of the radiative heat transfer; therefore, the developed Nusselt number correlations represent both radiative and convection heat transfer modes. Consequently, the radiative heat transfer has been taken indirectly into consideration in the calculations.

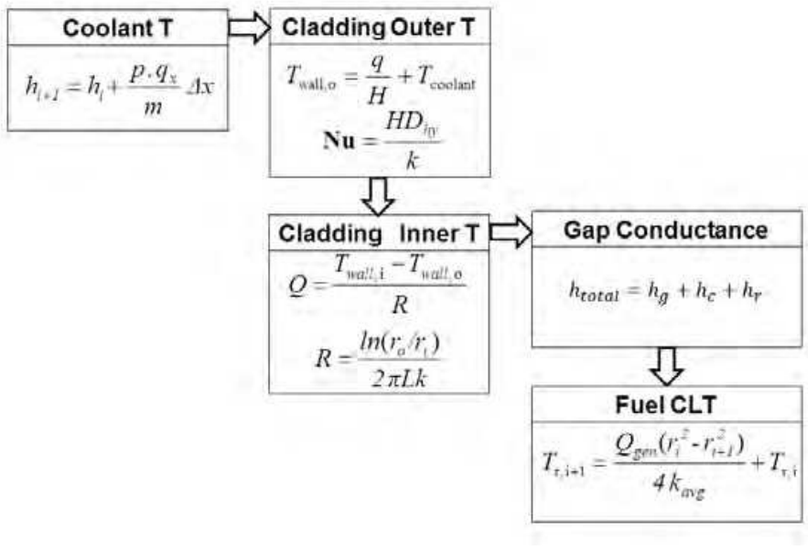

Fig. 12. Fuel centerline temperature calculations.

6.1 Bulk-fluid temperature profile

The temperature profile of the coolant along the heated length of the fuel channel can be calculated based on the heat balance. Equation (16) was used to calculate the temperature profile of the coolant. The NIST REPFROP software Version 8.0 was used to determine the thermophysical properties at a bulk-fluid temperature corresponding to each one-millimeter interval.

$$h_{i+1} = h_i + \frac{p \cdot q_x}{\dot{m}} \cdot \Delta x \tag{16}$$

In Eq. (16), q_x is the axial heat flux value, which is variable along the heated length of the fuel channel if a non-uniform Axial Heat Flux Profile (AHFP) is used. In the present chapter, four AHFPs have been applied in order to calculate the fuel centerline temperature in fuel channels at the maximum channel thermal power. These AHFPs are cosine, upstream-skewed cosine, downstream-skewed cosine, and uniform. The aforementioned AHFPs were calculated based on power profiles listed in Leung (2008) while the downstream-skewed AHFP was determined as the mirror image of the upstream-skewed AHFP. A local heat flux can be calculated by multiplying the average heat flux by the corresponding power ratio from Fig. 13.

It should be noted that there are many power profiles in a reactor core. In other words, the axial heat flux profile in each fuel channel differs from those of the other fuel channels. This variation in power profiles is due to the radial and axial power distribution, fuel burn-up, presence of reactivity control mechanisms, and refuelling scheme. Thus, a detailed design requires the maximum thermal power in the core, which can be determined based on neutronic analysis of the core which is beyond the scope of this chapter. However, the four examined AHFPs envelope a wide range of power profiles.

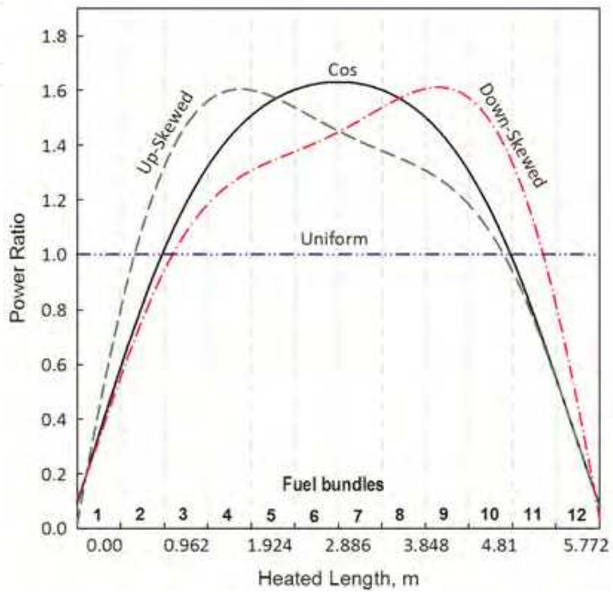

Fig. 13. Power ratios along heated length of fuel channel (based on Leung (2008)).

6.2 Sheath temperature

The calculation of the sheath temperature requires HTC values along the heated length of the fuel channel. In this study, the Mokry et al. correlation, shown as Eq. (17), has been used to determine HTC. The average Prandtl number in the Mokry correlation is calculated based on the average specific heat using Eq. (18). In Eq. (18) μ and k are the dynamic viscosity and thermal conductivity of the coolant at bulk temperature. The experimental data, based on which this correlation was developed, was obtained within conditions similar to those of proposed SCWR concepts. The experimental dataset was obtained for supercritical water flowing upward in a 4-m-long vertical bare tube. The data was collected at a pressure of approximately 24 MPa for several combinations of wall and bulk fluid temperatures. The temperatures were below, at, or above the pseudocritical temperature. The mass flux ranged from 200-1500 kg/m^{2}s; coolant inlet temperature varied from 320 to 350°C, for heat flux up to 1250 kW/m^2 (Mokry et al., 2009). The Mokry correlation requires iterations to be solved, because it contains two unknowns, which are HTC and sheath wall temperature. To solve this problem through iterations, Newton's law of cooling should be used.

From a safety point of view, it is necessary to know the uncertainty of a correlation in calculating the HTC and sheath wall temperature. As shown in Fig. 14, the uncertainty associated in the prediction of the HTC using the Mokry et al. correlation is ±25%. In other

words, the HTC values calculated by the Mokry correlation are within ±25% deviation from the corresponding experimental values. However, the uncertainty associated with wall temperature is smaller and lies within ±15%. Figure 15 shows the uncertainty in the prediction of the wall temperature associated with the Mokry et al. correlation.

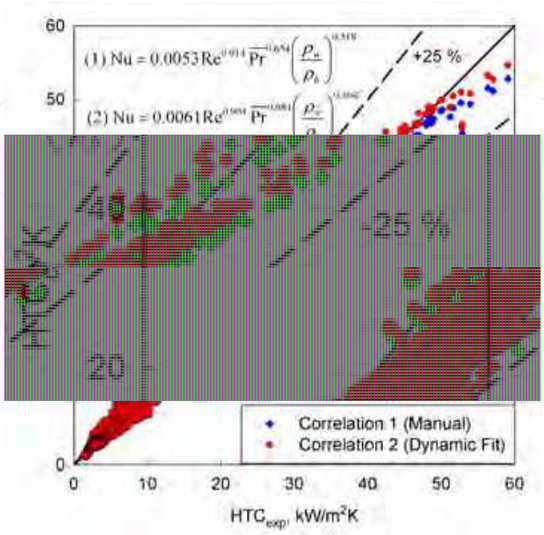

Fig. 14. Uncertainty in predicting HTC based on the Mokry et al. correlation (Mokry et al., 2011).

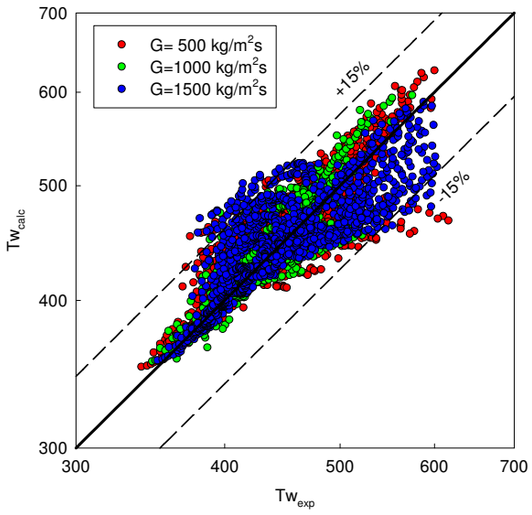

Fig. 15. Uncertainty in predicting wall temperature using the Mokry et al. correlation (Mokry et al., 2011).

6.2.1 Outer-surface temperature of sheath

The following sequence of equations can be used in order to calculate the outer surface temperature of the sheath along the heated length of the fuel channel.

Assumption to start the iteration: $T_{sheath,wall\,o} = T_{bulk} + 50^{\circ}\mathrm{C}$

$$\mathbf{Nu}_{\mathrm{b}} = 0.0061\,\mathbf{Re}_{\mathrm{b}}^{0.904}\,\overline{\mathbf{Pr}}_{\mathrm{b}}^{0.684}\left(\frac{\rho_w}{\rho_b}\right)^{0.564} \tag{17}$$

$$\overline{\mathbf{Pr}} = \frac{\mu \bar{c}_p}{k},\ \bar{c}_p = \frac{H_{sheath,T} - H_{bulk,T}}{T_{sheath} - T_{bulk}} \tag{18}$$

$$q = h\left(T_{sheath,wall\,o} - T_{bulk}\right) \tag{19}$$

The developed MATLAB code uses an iterative technique to determine the sheath-wall temperature. Initially, the sheath-wall temperature is unknown. Therefore, an initial guess is needed for the sheath-wall temperature (i.e., 50°C above the bulk-fluid temperature). Then, the code calculates the HTC using Eq. (17), which requires the thermophysical properties of the light-water coolant at bulk-fluid and sheath-wall temperatures. Next, the code calculates a "new" sheath-wall temperature using the Newton's law of cooling shown as Eq. (19). In the next iteration, the code uses an average temperature between the two consecutive temperatures. The iterations continue until the difference between the two consecutive temperatures is less than 0.1 K. It should be noted that the initial guessed sheath-wall temperature could have any value, because regardless of the value the temperature converges. The only difference caused by different guessed sheath-wall temperatures is in the number of iterations and required time to complete the execution of the code.

As mentioned previously, the thermophysical properties of the coolant undergo significant changes as the temperature passes through the pseudocritical point. Since the operating pressure of the coolant is 25 MPa, the pseudocritical point is reached at 384.9°C. As shown in Fig. 16, the changes in the thermophysical properties of the coolant were captured by the Nusselt number correlation, Eq. (16). The Prandtl number in Eq. (16) is responsible for taking into account the thermophysical properties of the coolant. Figure 16 shows the thermophysical properties of the light-water coolant along the length of the fuel channel. The use of these thermophysical properties in the Nusselt number correlation indicates that the correlation takes into account the effect of the pseudocritical point on the HTC between the sheath and the coolant.

6.2.2 Inner-sheath temperature

The inner surface temperature of the sheath can be calculated using Eq. (20). In Eq. (20), k is the thermal conductivity of the sheath, which is calculated based on the average temperature of the outer and inner wall surface temperatures. This inner-sheath temperature calculation is conducted through the use of an iteration, which requires an initial guess for the inner surface temperature of the sheath.

$$Q = \frac{T_{sheath,wall\,i} - T_{sheath,wall\,o}}{\frac{ln(r_o / r_i)}{2\pi L k}} \tag{20}$$

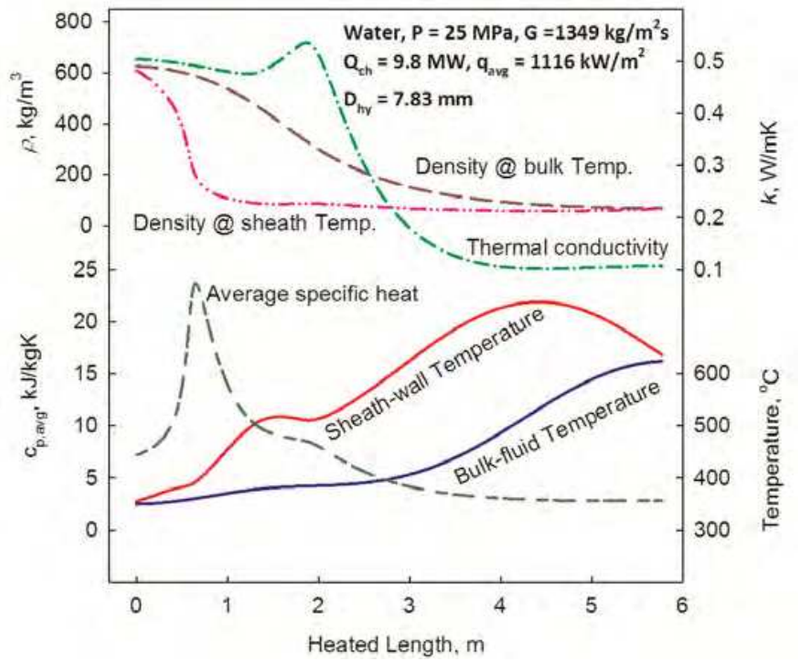

Fig. 16. Thermophysical properties of light-water coolant as function of temperature.

6.3 Gap conductance

Heat transfer through the fuel-sheath gap is governed by three primary mechanisms (Lee et al., 1995). These mechanisms are 1) conduction through the gas, 2) conduction due to fuel-sheath contacts, and 3) radiation. Furthermore, there are several models for the calculation of heat transfer rate through the fuel-sheath gap. These models include the offset gap conductance model, relocated gap conductance model, Ross and Stoute model, and modified Ross and Stoute model.

In the present study, the modified Ross and Stoute model has been used in order to determine the gap conductance effects on the fuel centerline temperature. In this model, the total heat transfer through the gap is calculated as the sum of the three aforementioned terms as represented in Eq. (21):

$$h_{total} = h_g + h_c + h_r \tag{21}$$

The heat transfer through the gas in the fuel-sheath gap is by conduction because the gap width is very small. This small gap width does not allow for the development of natural convection though the gap. The heat transfer rate through the gas is calculated using Eq. (22).

$$h_g = \frac{k_g}{1.5\,(R_1 + R_2) + t_g + g} \tag{22}$$

Where, h_g is the conductance through the gas in the gap, k_g is the thermal conductivity of the gas, R_1 and R_2 are the surface roughnesses of the fuel and the sheath, and t_g is the circumferentially average fuel-sheath gap width.

The fuel-sheath gap is very small, in the range between 0 and 125 μm (Lassmann and Hohlefeld, 1987). CANDU reactors use collapsible sheath, which leads to small fuel-sheath gaps approximately 20 μm (Lewis et al., 2008). Moreover, Hu and Wilson (2010) have reported a fuel-sheath gap width of 36 μm for a proposed PV SCWR. In the present study, the fuel centerline temperature has been calculated for both 20-μm and 36-μm gaps. In Eq. (22), g is the temperature jump distance, which is calculated using Eq. (23) (Lee et al., 1995).

$$\frac{1}{g} = \sum_i \left[\frac{y_i}{g_{o,i}} \right] \left(\frac{T_g}{273.15} \right)^{s+0.5} \left(\frac{0.101}{P_g} \right) \tag{23}$$

Where, g is the temperature jump distance, y_i is the mole fraction of the i_{th} component of gas, $g_{o,i}$ is the temperature jump distance of the i_{th} component of gas at standard temperature and pressure, T_g is the gas temperature in the fuel-sheath gap, P_g is the gas pressure in the fuel-sheath gap, and s is an exponent dependent on gas type.

In reality, the fuel pellets become in contact with sheath creating contact points. These contact points are formed due to thermal expansion and volumetric swelling of fuel pellets. As a result, heat is transferred through these contact points. The conductive heat transfer rate at the contact points are calculated using Eq. (24) (Ainscough, 1982). In Eq. (24), A is a constant, P_a is the apparent interfacial pressure, H is the Mayer hardness of the softer material. A and n are equal to 10 and 0.5.

$$h_c = A \frac{2k_f \, k_{sheath}}{(k_f + k_{sheath}) \left[\left(R_f^2 + R_{sheath}^2 \right) / 2 \right]^{1/2}} \left(\frac{P_a}{H} \right)^n \tag{24}$$

The last term in Eq. (21) is the radiative heat transfer coefficient through the gap, which is calculated using Eq. (25) (Ainscough, 1982). It should be noted that the contribution of this heat transfer mode is negligible under normal operating conditions. However, the radiative heat transfer is significant in accident scenarios. Nevertheless, the radiative heat transfer through the fuel-sheath gap has been taken into account in this study. In Eq. (25), ε_f and ε_{sheath} are surface emissivities of the fuel and the sheath respectively; and temperatures are in degrees Kelvin.

$$h_r = \frac{\sigma \varepsilon_f \, \varepsilon_{sheath}}{\varepsilon_f + \varepsilon_{sheath} - \varepsilon_f \, \varepsilon_{sheath}} \cdot \frac{\left(T_{f,o}^4 - T_{sheath,i}^4 \right)}{\left(T_{f,o} - T_{sheath,i} \right)} \tag{25}$$

6.4 Fuel centerline temperature

Equation (26) can be used to calculate the fuel centerline temperature. The thermal conductivity in Eq. (26) is the average thermal conductivity, which varies as a function of temperature. In order to increase the accuracy of the analysis, the radius of the fuel pellet has been divided into 20 rings. Initially, the inner-surface temperature is not known, therefore, an iteration loop should be created to calculate the outer-surface temperature of the fuel and the thermal conductivity of the fuel based on corresponding average temperatures.

$$T_{r,i+1} = \frac{Q_{gen}\left(r_i^2 - r_{i+1}^2\right)}{4 \cdot k_{avg}} + T_{r,i} \tag{26}$$

7. Results: Fuel centerline and sheath temperatures

There are two temperature limits that a fuel and a fuel bundle must meet. First, the sheath temperature must not exceed the design limit of 850°C (Chow and Khartabil, 2008). Second, when UO_2 fuel is used, the fuel centerline temperature must be below the industry accepted limit of 1850°C (Reisch, 2009) at all normal operating conditions.

Previously, it was mentioned that the industry accepted temperature limit for UO_2 fuel is 1850°C; however, this temperature limit might be different for fuels other than UO_2. There are several factors that may affect a fuel centerline temperature limit for a fuel. These factors include melting point, high-temperature stability, and phase change of the fuel. For instance, the accepted fuel centerline temperature limit of UO_2 fuel is approximately 1000°C below its melting point. As a result, the same fuel centerline temperature limit has been established for the other low thermal-conductivity fuels and enhanced thermal-conductivity fuels. In regards to ThO_2, the melting point is higher than that of UO_2, but a high uncertainty is associated with its melting point. Therefore, as a conservative approach, the same temperature limit has been established for ThO_2. Similarly, the corresponding limit for UC fuel would be 1500°C, because the melting point of UC is approximately 2505°C. UN fuel decomposes to uranium and gaseous nitrogen at temperatures above 1600°C. Therefore, the fuel centerline temperature limit for UN should be lower than that of UO_2 under normal operating conditions. Ma (1983) recommends a temperature limit of 1500°C for UN.

A steady-state one-dimensional heat transfer analysis was conducted in order to calculate the fuel centerline temperature at SCW fuel channels. Based on the proposed core configuration SCW fuel channels are located at the center of the core. Consequently, the thermal power in some of these fuel channels might be by a factor higher than the average channel power of 8.5 MW_{th}. Therefore, in the present study, a thermal power per channel of 9.8 MW_{th} has been considered for the SCW fuel channels with the maximum thermal power. This thermal power is approximately 15% (i. e. 10% above the average power and 5% uncertainty) above the average thermal power per channel. The conditions based on which the calculations have been conducted are as follows: an average mass flow rate of 4.4 kg/s, a constant pressure of 25 MPa, a coolant inlet temperature of 350°C, a thermal power per channel of 9.8 MW_{th}.

The presented analysis does not take into account the pressure drop of the coolant. The main reason for not taking the pressure drop into consideration is that the pressure drop is inversely proportional to the square of mass flux. In a CANDU fuel channel, the pressure drop is approximately 1.75 MPa (AECL, 2005). In addition, the mass flux in an SCWR fuel channel is approximately 5 times lower than that of a CANDU reactor. Therefore, the pressure drop of a SCWR fuel channel should be significantly lower than 1.75 MPa. As a result, the pressure drop has not been taken into consideration.

In addition, this study does not determine the sheath and the fuel centerline temperatures for the SRH fuel channels mainly due to the fact that the average thermal power in SRH channels is 5.5 MW_{th} (see Table 1). Since the thermal power in SRH channels is

approximately 35% less that of the SCW channels, the sheath and the fuel centerline temperatures will be definitely lower than those of the SCW channels. As a result, if a fuel and sheath meet their corresponding temperature limits under the operating conditions of the SCW channels with the maximum thermal power, they will be suitable for the SRH channels as well.

For the SCW fuel channels, the fuel centreline temperature has been calculated at cosine, upstream-skewed cosine, downstream-skewed cosine, and uniform axial heat flux profiles. These heat flux profiles have been calculated based on the Variant-20 fuel bundle. Each of the 42 fuel elements of the Variant-20 fuel bundle has an outer diameter of 11.5 mm while the minimum required thickness of the sheath has been determined to be 0.48 mm. Therefore, the inner diameter of the sheath is 10.54 mm. Inconel-600 was chosen as the material of the sheath.

The examined fuels were UO_2, MOX, ThO_2, UC, UN, UO_2-SiC, UO_2-C, and UO_2-BeO. For each fuel, the fuel centerline temperature was analysed at the aforementioned AHFPs. Since the maximum fuel centerline temperature was reached at downstream-skewed cosine AHFP for all the examined fuels, only the results associated with this AHFP have been presented in this section. Figures 17 through 19 show the coolant, sheath, and fuel centerline temperature profiles as well as the heat transfer coefficient profile along the heated length of the fuel channel for UO_2, UC, and UO_2-BeO fuels. Each of these three fuels represents one fuel category (i.e., low, enhanced, high thermal-conductivity fuels). It should be noted that the results presented in Figs. 17 through 19 are based on a 20-μm fuel-sheath gap.

In addition, Figure 20 shows the maximum fuel centerline temperatures of all the examined fuels. As shown in Figure 20, the maximum fuel centerline temperatures of all examined low thermal-conductivity fuels exceed the temperature limit of 1850°C. On the other hand, enhanced thermal-conductivity fuels and high thermal-conductivity fuels show fuel centerline temperatures below the established temperature limits of 1850°C and 1500°C, respectively.

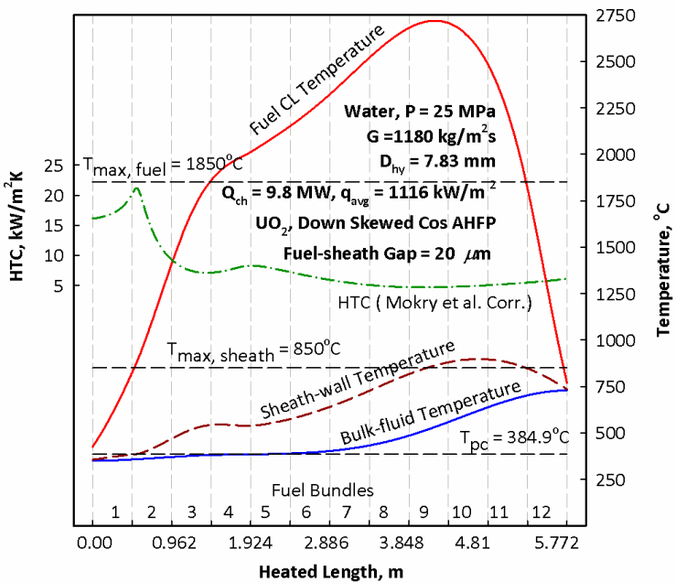

Fig. 17. Temperature and HTC profiles for UO_2 at downstream-skewed cosine AHFP.

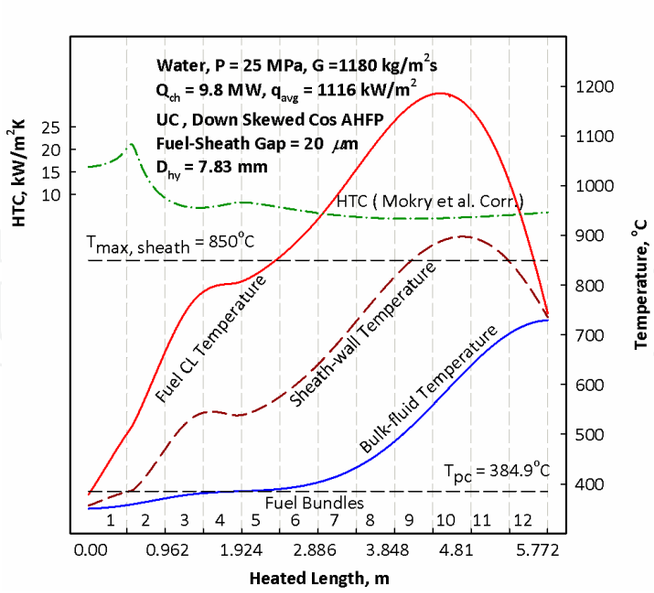

Fig. 18. Temperature and HTC profiles for UC at downstream-skewed cosine AHFP.

In regards to sheath temperature, the sheath temperature reached its maximum at downstream-skewed cosine AHFP. Figure 21 provides a comparison between the sheath temperature profiles for the four studied AHFPs. Figure 21 also shows the HTC profiles corresponding to each examined AHFPs. As shown in Fig. 21, unlike uniform AHFP, HTC reaches its maximum value in the beginning of the fuel channel for non-uniform AHFPs (i.e., downstream-skewed cosine, cosine, and upstream-skewed cosine AHFPs). This increase in HTC is due to the fact the sheath temperature reaches the pseudocritical temperature. In contrast, with uniform AHFP, the sheath temperature is above the pseudocritical temperature from the inlet of the fuel channel. Consequently, the peak in HTC at uniform AHFP occurs when the coolant reaches the pseudocritical temperature.

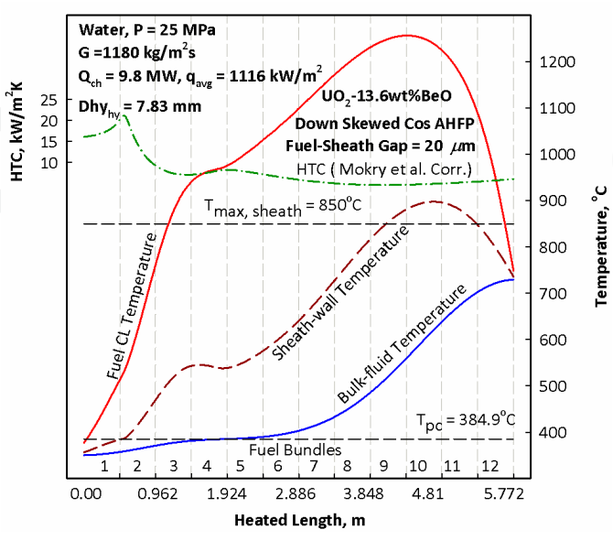

Fig. 19. Temperature and HTC profiles for UO_2–BeO at downstream-skewed cosine AHFP.

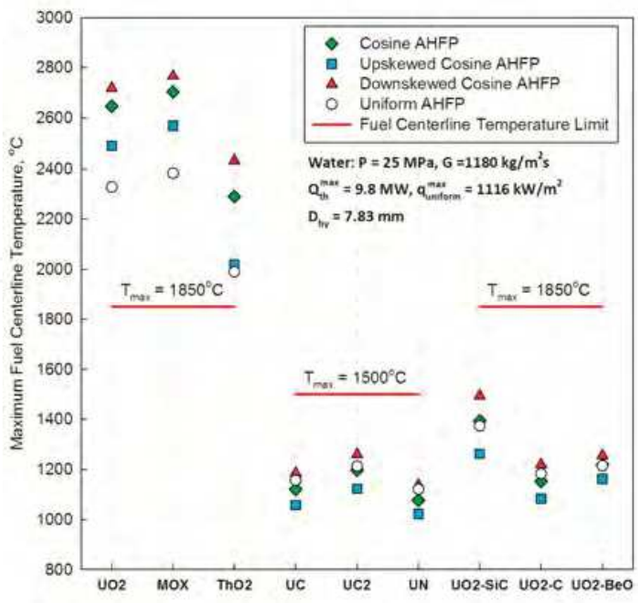

Fig. 20. Maximum fuel centerline temperatures of examined fuels based on a 20–μm fuel-sheath gap width.

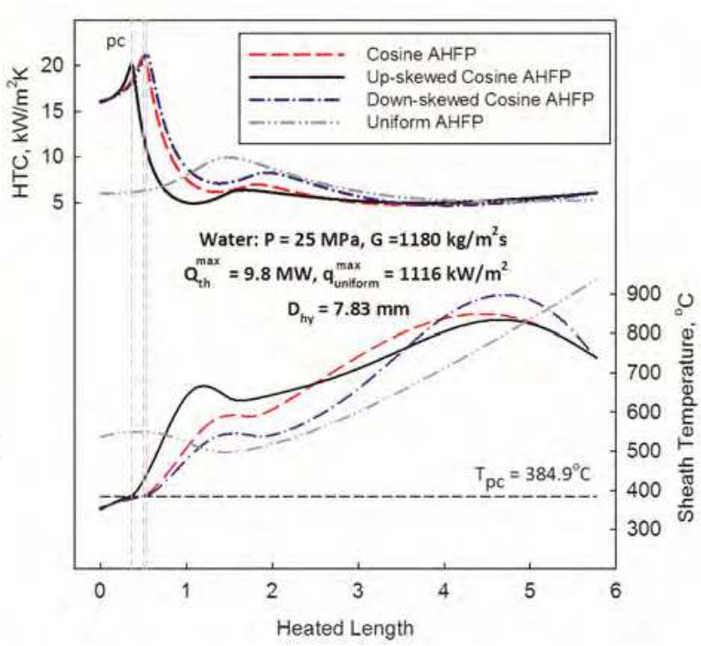

Fig. 21. HTC and sheath-wall temperature profiles as function of AHPF.

A comparison between the examined non-uniform AHFPs shows that in terms of the sheath and fuel centerline temperatures, upstream-skewed cosine AHFP is the most ideal heat flux profile. On the other hand, the downstream-skewed cosine AHFP results in the highest temperatures. Thus, for design purposes, it is a conservative approach to determine the sheath and fuel centerline temperatures based on a downstream-skewed AHFP.

8. Conclusion

Since the development of SCWRs is still in the conceptual design stage, it is worth to further investigate heat transfer and neutronic aspects of high and enhanced thermal-conductivity fuels. In regards to high thermal-conductivity and enhanced thermal-conductivity fuels, this study recommends the use of UC and UO_2-BeO, respectively. This use is conditional on the assurance of chemical compatibility, mechanical behavior, and irradiation behavior of these fuels under the SCWR conditions. In addition, the development of new fuel bundle designs, which will comply with the design temperature limits on the fuel and the sheath, is necessary. New fuel-bundle designs, which would result in lower fuel centerline temperatures, also allow for the use of low thermal-conductivity fuels.

Heat transfer at supercritical conditions has been studied by many researchers; however, still there is a need to improve the correlations used to predict the heat transfer coefficient. To the knowledge of the authors, none of the available heat-transfer correlations predicts the deteriorated heat transfer regime. The lack of capability to predict such phenomenon may result in melting of the sheath. Thus, it is significantly important to develop either look-up tables or heat transfer correlations that would predict the deteriorated heat transfer regime.

9. Acknowledgment

Financial supports from the NSERC/NRCan/AECL Generation IV Energy Technologies Program and NSERC Discovery Grant are gratefully acknowledged.

10. References

AECL (2005). CANDU 6 Technical Summary. CANDU 6 Program Team Reactor Development Business Unit.

Ainscough, J. B. (1982). Gap conductance in Zircaloy-Clad LWR Fuel Rods.United Kingdom Atomic Energy Authority.

Bae, Y.-Y., Kim, H.-Y., and Kang, D-J (2010). Forced and Mixed Convective Heat Transfer to CO_2 at a Supercritical Pressure Vertically Flowing in a Uniformly-Heated Circular Tubes. Experimental Thermal and Fluid Science, Vol. 34, 1295-1308.

Bae, Y.-Y., and Kim, H.-Y. (2009). Convective Heat Transfer to CO_2 at a Supercritical Pressure Flowing Vertically Upward in Tubes and an Annular Channel. Experimental Thermal and Fluid Science, Vol. 33, No. 2, 329-339.

Balankin, S. A., Loshmanov, L. P., Skorov, D. M., and Skolov, V. S. (1978).Thermodynamic Stability of Uranium Nitride. J. Atomic Energy 44, No. 4, 327-329.

Bishop, A. A., Sandberg, R. O., and Tong, L.S. (1965), Forced Convection Heat Transfer to Water at Near-critical Temperatures and Supercritical Pressures, A.I.Ch.E.-I.Chem.E Symposium Series No. 2, 77−85.

Bowman, A. L., Arnold, G. P., Witteman, W. G., and Wallace, T. C. (1966). Thermal Expansion of Uranium Dicarbide and Uranium Sesquicarbide. J. Nuclear Materials 19, 111-112.

Carbajo, J. J., Yoder, G. L., Popov, S. G., and Ivanov, V. K. (2001). A Review of the Thermophysical Properties of MOX and UO2 Fuels. J. Nuclear Materials 299, 181-198.

Chow, C. K., and Khartabil, H.F. (2008). Conceptual Fuel Channel Designs for CANDU-SCWR. J. Nuclear Engineering and Technology 40, 1−8.

Cochran, R. G., and Tsoulfanidis, N. (1999). The Nuclear Fuel Cycle: Analysis and Management. Second ed. American Nuclear Society, Illinois, USA.

Coninck, R. D., Lierde, W. V., and Gijs, A. (1975). Uranium Carbide: Thermal Diffusivity, Thermal Conductivity Spectral Emissivity at High Temperature. J. Nuclear Materials 57, 69-76.

Coninck, R. D., Batist, R. D., and Gijs, A. (1976). Thermal Diffusivity, Thermal Conductivity and Spectral Emissivity of Uranium Dicarbide at High Temperatures. J. Nuclear Materials 8, 167-176.

Cox, D., and Cronenberg, A. (1977). A Theoretical Prediction of the Thermal Conductivity of Uranium Carbide Vapor. J. Nuclear Materials 67, 326-331.

Diamond, W. T. (2010). Development of Out-of-Core Concepts for a Supercritical-Water, Pressure-Tube Reactor. Proc. 2nd Canada-China Joint Workshop on Supercritical Water-Cooled Reactors (CCSC-2010), Toronto, Ontario, Canada: Canadian Nuclear Society, April 25-28, 15 pages.

Farah, A., King, K., Gupta, S., Mokry, S., and Pioro, I. (2010). Comparison of Selected Heat-Transfer Correlations for Supercritical Water Flowing Upward in Vertical Bare Tubes. Proc. 2nd Canada-China Joint Workshop on Supercritical Water-Cooled Reactors (CCSC-2010), Toronto, Ontario, Canada: Canadian Nuclear Society, April 25-28, 12 pages.

Frost, B. R. (1963). The Carbides of Uranium. J. Nuclear Materials 10, 265-300.

Gabaraev, B.A., Vikulov, V.K., and Yermoshin, F.Ye. et al. (2004). Pressure tube once-through reactor with supercritical coolant pressure, (In Russian). Proceedings of the International Scientific-Technical Conference "Channel Reactors: Problems and Solutions", Moscow, Russia, October 19–22, Paper #42.

Gingerich, K. A. (1969). Vaporization of Uranium.Mononitride and Heat of Sublimation of Uranium. J. Chemical Physics 51, No. 10, 4433-4439.

Gnielinski, V. (1976). New Equation for Heat and Mass Transfer in Turbulent Pipe and Channel Flow, Intern. Chem. Eng., Vol. 16, No. 2, 359-366.

Grabezhnaya, V. A., and Kirillov, P. L. (2006). Heat Transfer at Supercritical Pressuresand Heat Transfer Deterioration Boundaries. Thermal Engineering , Vol. 53, No. 4, 296–301.

Grande, L., Mikhael, S., Villamere, B., Rodriguez-Prado, A., Allison, L., Peiman W. and Pioro, I. (2010). Thermal Aspects of Using Uranium Nitride in Supercritical Water-Cooled Nuclear Reactors, Proceedings of the 18th International Conference On Nuclear Engineering (ICONE-18), Xi'an, China.

Griem, H. (1996). A New Procedure for the Near-and Supercritical Prediction Pressure of Forced Convection Heat Transfer, Heat Mass Trans., Vol. 3, 301–305.

Groom (2003). Annulus Gas Chemistry Control. International Atomic Energy Agency. Karachi Nuclear Power Plant (KANUPP), Karachi. 19 May 2008 <http://canteach.candu.org/library/20032103.pdf>.

Harrison, J. W. (1969). The Irradiation-Induced Swelling of Uranium Carbide. J. Nuclear Materials 30, 319-323.

Hayes, S., Thomas, J., and Peddicord, K. (1990a). Material Properties of Uranium Mononitride-III Transport Properties. J. Nuclear Materials 171, 289-299.

Hayes, S., Thomas, J., and Peddicord, K. (1990b). Material Property Correlations for Uranium Mononitride-II Mechanical Properties. J. Nuclear Materials 171, 271-288.

Hayes, S., Thomas, J., Peddicord, K. (1990c). Material Property Correlations for Uranium Mononitride-IV Thermodynamic Properties. J. Nuclear Materials 171, 300-318.

Hollenbach, D. F., and Ott, L. J. (2010). Improving the Thermal Conductivity of UO2 Fuel with the Addition of Graphite Fibers, Transactions of the American Nuclear Society and Embedded Topical Meeting "Nuclear Fuels and Structural Materials for the Next Generation Nuclear Reactors", San Diego, California, June 13-17, 485-487.

Hu, L., Wang, C., Huang, Y. (2010). Porous Yttria-Stabilized Zirconia Ceramics with Ultra-Low Thermal Conductivity. J. of Materials Science 45, 3242-3246.

Hu, P. and Wilson, P. P. H. (2010). Supercritical Water Reactor Steady-State, Burn-up, and Transient Analysis with Extended PARCS/RELAP5. Journal of Nuclear Technology, Vol. 172, 143-156.

IAEA (2005). Thorium Fuel Cycle — Potential Benefits and Challenges. Retrieved March 9, 2011, from IAEA: http://www-pub.iaea.org/mtcd/publications/pdf/te_1450_web.pdf .

IAEA (2006). Thermophysical properties database of materials for light water reactors and heavy water reactors. Vienna, Austria.

IAEA (2008). Thermophysical Properties of Materials for Nuclear Engineering: A Tutorial and Collection of Data. Vienna, Austria.

Incropera, F. P., Dewitt, D. P., Bergman, T. L., and Lavine, A. S. (2006). Fundamentals of Heat and Mass Transfer, sixth ed. Wiley, USA.

INSC. Thermal Conductivity of Solid UO_2. Retrieved June 28, 2010, from International Nuclear Safety Center (INSC, 2010): http://www.insc.anl.gov/matprop/uo2/cond/solid/index.php.

Jackson, J. D. (2002). Consideration of the Heat Transfer Properties of Supercritical Pressure Water in Connection With the Cooling of Advanced Nuclear Reactors, Proc. of the 13th Pacific Basin Nuclear Conference Shenzhen City, China, 21–25 October.

Jain, D., Pillai, C., Rao, B. K., and Sahoo, K. (2006). Thermal Diffusivity and Thermal Conductivity of Thoria-Lanthana Solid Solutions up to 10 mol.% LaO (1.5), J. of Nuclear Materials 353, 35-41.

Khan, J. A., Knight, T. W., Pakala, S. B., Jiang, W., and Fang, R. (2010). Enhanced Thermal Conductivity for LWR Fuel. J. Nuclear Technology 169, 61-72.

Kikuchi, T., Takahashi, T., and Nasu, S. (1972). Porosity Dependence of Thermal Conductivity of Uranium Mononitride. J. Nuclear Materials 45, 284-292.

Kirillov, P.L., Terent'eva, M.I., and Deniskina, N.B. (2007). Thermophysical Properties of Nuclear Engineering Materials, third ed. revised and augmented, IzdAT Publ. House, Moscow, Russia, 194 pages.

Krasnoshchekov, E. A., and Protopopov, V. S. (1966). Experimental Study of Heat Exchange in Carbon Dioxide in the Supercritical Range at High Temperature Drops, Teplofizika Vysokikh Tempraturi (High Temp.), Vol. 4, No. 3.

Kuang, B., Zhang, Y., and Cheng, X. (2008). A New, Wide-Ranged Heat Transfer Correlation of Water at Supercritical Pressures in Vertical Upward Ducts, NUTHOS-7, Seoul, Korea, October 5–9.

Kutz, M. (2005). Mechanical Engineers' Handbook, Materials and Mechanical Design, 3rd Edition, John Wiley and Sons.

Lassmann, K. and Hohlefeld, F. (1987). The Revised Gap Model to Describe the Gap Conductance between Fuel and Cladding. Journal of Nuclear Engineering and Design 103, 215-221.

Lee, K. M., Ohn, M. Y., Lim, H. S., Choi, J. H., and Hwang, S. T. (1995). Study on Models for Gap Conductance between Fuel and Sheath for CANDU Reactors. Journal of Ann. Nucl. Energy, Vol. 22, No. 9, 601-610.

Leitnaker, J. M. and Godfrey, T. G. (1967). Thermodynamic Properties of Uranium Carbide. J. Nuclear Materials 21, 175-189.

Leung, L. K. H. (2008). Effect of CANDNU Bundle-Geometry Variation on Dryout Power. Proc. ICONE-16, Orlando, USA, Paper #48827, 8 pages.

Lewis, B.J., Iglesias, F.C., Dickson, R.S., and Williams, A. (2008). Overview of High Temperature Fuel Behaviour. 10th CNS International Conference on CANDU Fuel, Ottawa, Canada, October 5-8.

Liu, X.J., Yang, T., and Cheng X. (2010). Core and Sub-Channel Analysis of SCWR with Mixed Spectrum Core. Ann. Nucl. Energy, doi: 10.1016/ j.anucene.2010.07.014.

Lundberg, L. B., and Hobbins, R. R. (1992). Nuclear Fuels for Very High Temperature Applications. Intersociety Energy Conversion Engineering Conf., San Diego, 9 pages.

Ma, B. M. (1983). Nuclear Reactor Materials and Applications. Van Nostrand Reinhold Company Inc., New York.

Maxwell, J. C. (1954). Treatise on electricity and magnetism. Dover Publications.

Matthews, R. B., Chidester, K. M., Hoth, C. W., Mason, R. E., and Petty, R. L. (1988). Fabrication and Testing of Uranium Nitride Fuel for Space Power Reactors. J. Nuclear Materials 151, 334–344.

Mokry, S., Pioro, I.L., Farah, A., King, K., Gupta, S., Peiman, W. and Kirillov, P. (2011). Development of Supercritical Water Heat-Transfer Correlation for Vertical Bare Tubes, Nuclear Engineering and Design, Vol. 241, 1126-1136.

Mokry, S., Gospodinov, Ye., Pioro, I. and Kirillov, P.L. (2009). Supercritical Water Heat-Transfer Correlation for Vertical Bare Tubes. Proc. ICONE-17, July 12-16, Brussels, Belgium, Paper #76010, 8 pages.

Naidin, M., Monichan, R., Zirn, U., Gabriel, K. and Pioro, I. (2009). Thermodynamic Considerations for a Single-Reheat Cycle SCWR, Proc. ICONE-17, July 12-16, Brussels, Belgium, Paper #75984, 8 pages.

Naidin, M., Pioro, I., Duffey, R., Zirn, U., and Mokry, S. (2009). SCW NPPs: Layouts and Thermodynamic Cycles Options. Proc. Int. Conf. "Nuclear Energy for New Europe", Bled, Slovenia, Sep. 14-17, Paper #704, 12 pages.

Naterer, G., Suppiah, S., Lewis, M. (2009). Recent Canadian Advances in Nuclear-Based Hydrogen Production and the Thermochemical Cu-Cl Cycle, Int. J. of Hydrogen Energy (IJHE), Vol. 34, 2901-2917.

Naterer, G.F., Suppiah, S., Stolberg, L., et al. (2010). Canada's Program on Nuclear Hydrogen Production and the Thermochemical Cu-Cl Cycle, Int. J. of Hydrogen Energy (IJHE), Vol. 35, 10905-10926.

National Institute of Standards and Technology (2007). NIST Reference Fluid Thermodynamic and Transport Properties-REFPROP. NIST Standard Reference Database 23, Ver. 8.0. Boulder, CO, U.S.: Department of Commerce.

OECD Nuclear Energy Agency. (2010). Lead-Cooled Fast Reactor. Retrieved April 2, 2011, from Generation IV Technologies:
http://www.gen-4.org/Technology/systems/lfr.htm.

Oggianu, S. M., No, H. C., and Kazimi, M. (2003). Analysis of Burnup and Economic Potential of Alternative Fuel Materials in Thermal Reactors. j. Nuclear Technology 143, 256-269.

Oka, Y., Koshizuka, S., Ishiwatari, Y., Yamaji, A. (2010). Super Light Water Reactors and Super Fast Reactors: Supercritical-Pressure Light Water Cooled Reactors. Springer, New York.

Pioro, I. L., and Duffey, R. B. (2007). Heat Transfer and Hydraulic Resistance at Supercritical Pressure in Power-Engineering Applications. ASME, New York.

Pioro, I., Mokry, S., Peiman, W., Grande, L., and Saltanov, Eu. (2010). Supercritical Water-Cooled Nuclear Reactors: NPP Layouts and Thermal Design Options of Pressure Channels. Proceedings of the 17th Pacific Basin Nuclear Conference (PBNC-2010), Cancun, Mexico.

Reisch, F. (2009). High Pressure Boiling Water Reactor, HP-BWR. Royal Institute of Technology, Nuclear Power Safety, Stockholm, Sweden.

Ross, S. B., El-Genk, M. S., and Matthews, R. B. (1988). Thermal Conductivity Correlation for Uranium Nitride Fuel. J. Nuclear Materials 151, 313-317.

Ross, S. B., El-Genk, M. S., and Matthews, R. B. (1990). Uranium nitride fuel swelling correlation. J. Nuclear Materials 170, 169-177.

Routbort, J. L. (1972). High-Temperature Deformation of Polycrystalline Uranium Carbide. J. Nuclear Materials 44, 24-30.

Routbort, J. L., and Singh, R. N. (1975). Carbide and Nitride Nuclear Fuels. J. Nuclear Materials 58, 78-114.

Saltanov, E., Monichan, R., Tchernyavskaya, E., and Pioro, I. (2009). Steam-Reheat Option for SCWRs. Proc. ICONE-17, July 12-16, Brussels, Belgium, Paper #76061, 10 pages.

Schlichting, K. W., Padture, N. P., Klemens, P. G. (2001). Thermal conductivity of dense and porous yttria-stabilized zirconia.J. of Materials Science 31, 3003-3010.

Seltzer, M. S., Wright, T. R., and Moak, D. P. (1975). Creep Behavior of Uranium Carbide-Based Alloys. J. American Ceramic Society 58, 138-142.

Shoup, R. D., and Grace, W. R., (1977). Process Variables in the Preparation of UN Microspheres. J. American Ceramic Society 60, No. 7-8, 332-335.

Special Metals.(n.d.). Inconel alloy 600. Retrieved December 2, 2008, from http://www.specialmetals.com/products/inconelalloy600.php.

Stellrecht, D. E., Farkas, M. S., and Moak, D. P. (1968). Compressive Creep of Uranium Carbide. J. American Ceramic Society 51, No. 8, 455-458.

Tokar, M., Nutt, A. W., and Leary, J. A., (1970). Mechanical Properties of Carbide and Nitride Reactor Fuels. J. Reactor Technology. http://www.osti.gov/bridge/purl.cover.jsp?purl=/4100394-tE8dXk/.

U.S. DOE Nuclear Energy Research Advisory Committee (2002). A Technology Roadmap for Generation IV Nuclear Energy Systems. Retrieved July 12, 2010, from The Generation IV International Forum: http://www.ne.doe.gov/genIV/documents/gen_iv_roadmap.pdf.

Villamere, B., Allison, L., Grande, L., Mikhael, S., Rodriguez-Prado, A., and Pioro, I. (2009). Thermal Aspects for Uranium Carbide and Uranium Dicarbide Fuels in Supercritical Water-cooled Nuclear Reactors. Proc. ICONE-17, Brussels, Belgium, July 12-16, Paper #75990, 12 pages.

Wang, S., Yuan, L. Q., and Leung, L. K. (2010). Assessment of Supercritical Heat-Transfer Correlations against AECL Database for Tubes. Proc. 2nd Canada-China Joint Workshop on Supercritical Water-Cooled Reactors (CCSC-2010), Toronto, Ontario, Canada: Canadian Nuclear Society, April 25-28, 12 pages.

Wang, Z., Naterer, G. F., and Gabriel, K. S. (2010). Thermal Integration of SCWR Nuclear and Thermochemical Hydrogen Plants. Proc. 2nd Canada-China Joint Workshop on Supercritical Water-Cooled Reactors (CCSC-2010), Toronto, Ontario, Canada: Canadian Nuclear Society, April 25-28, 12 pages.

Watts, M. J., and Chou, C-T. (1982), Mixed Convection Heat Transfer to Supercritical Pressure Water, Proc. 7th, IHTC, Munich, Germany, 495–500.

Wheeler, M. J. (1965). Thermal Diffusivity at Incandescent Temperatures by a Modulated Electron Beam Technique. Brit. J. Appl. Phys., Vol. 16, 365-376.

Zahlan, H., Groeneveld, D., and Tavoularis, S., Mokry, S., Pioro, I. (2011). Assessment of Supercritical Heat Transfer Prediction Methods. Proc. of the 5th International Symposium on Supercritical Water-Cooled Reactors (ISSCWR-5), Vancouver, British Colombia, Canada, March 13-16.

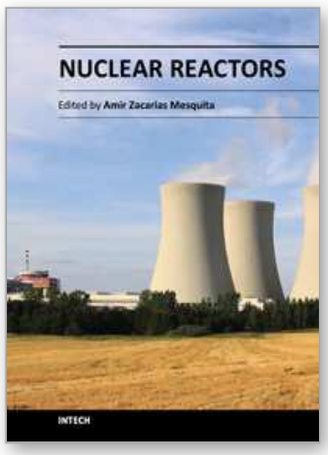

Nuclear Reactors

Edited by Prof. Amir Mesquita

ISBN 978-953-51-0018-8
Hard cover, 338 pages
Publisher InTech
Published online 10, February, 2012
Published in print edition February, 2012

This book presents a comprehensive review of studies in nuclear reactors technology from authors across the globe. Topics discussed in this compilation include: thermal hydraulic investigation of TRIGA type research reactor, materials testing reactor and high temperature gas-cooled reactor; the use of radiogenic lead recovered from ores as a coolant for fast reactors; decay heat in reactors and spent-fuel pools; present status of two-phase flow studies in reactor components; thermal aspects of conventional and alternative fuels in supercritical water?cooled reactor; two-phase flow coolant behavior in boiling water reactors under earthquake condition; simulation of nuclear reactors core; fuel life control in light-water reactors; methods for monitoring and controlling power in nuclear reactors; structural materials modeling for the next generation of nuclear reactors; application of the results of finite group theory in reactor physics; and the usability of vermiculite as a shield for nuclear reactor.

InTech Europe
University Campus STeP Ri
Slavka Krautzeka 83/A
51000 Rijeka, Croatia
Phone: +385 (51) 770 447
Fax: +385 (51) 686 166
www.intechopen.com

InTech China
Unit 405, Office Block, Hotel Equatorial Shanghai
No.65, Yan An Road (West), Shanghai, 200040, China
中国上海市延安西路65号上海国际贵都大饭店办公楼405单元
Phone: +86-21-62489820
Fax: +86-21-62489821

IntechOpen